Desalination and Water Treatment
www.deswater.com

doi: 10.5004/dwt.2021.27245

227 (2021) 188–215
July

Effect of the presence of metals on the adsorption and desorption of phenol on activated mangrove charcoal

Mohamed F. Sabbagh, Muhammad H. Al-Malack*

Department of Civil and Environmental Engineering, King Fahd University of Petroleum and Mineral, Dhahran 31261, Saudi Arabia, Tel. +966138604735; Fax: +966138602789; emails: mhmalack@kfupm.edu.sa (M.H. Al-Malack), g201704190@kfupm.edu.sa (M.F. Sabbagh)

Received 17 November 2020; Accepted 19 March 2021

ABSTRACT

Singular and competitive adsorption of phenol, Pb(II), Cr(III), and Cd(II) were studied using activated charcoal (AC) produced from mangrove charcoal, where KOH, $ZnCl_2$, and H_3PO_4 were used as activation agents. Raw and activated charcoal samples were characterized using elemental analysis, X-ray fluorescence, thermogravimetric, X-ray diffraction spectrometer, surface area analysis (Brunauer–Emmett–Teller), Fourier transform infrared spectroscopy, and scanning electron microscopy coupled with energy-dispersive X-ray spectroscopy. According to the obtained results, showed that the best prepared AC sample had a specific surface area of 784.29 m^2/g, when KOH was utilized at activation temperature and time of 600°C and 60 min, respectively. Effects of initial pH, adsorbent dosage, initial concentration, and contact time were studied in a singular system. The results showed that the maximum adsorption capacity at optimum conditions was around 41.5, 89.4, 34.2, and 25.2 mg/g of phenol, Pb, Cr, and Cd, respectively. In the binary system, phenol concentration, pH, and AC dosage were fixed at 50 mg/L, 5, and 1.25 g/L, respectively, where the AC was found to have a higher affinity to Pb (in phenol with Pb) and to phenol (in phenol Cr and Cd). Experimental data on the adsorption of phenol was found to fit the Freundlich isotherm model best, while heavy metals best fitted Langmuir isotherm. Furthermore, chemisorption was the attributed adsorption mechanism, since the equilibrium data best fitted the pseudo-second-order kinetic model. The regeneration study revealed that phenol removal efficiency dropped by 13.6% after three cycles using NaOH while using HCl the drop was 43.3%.

Keywords: Activation agent; Competitive adsorption; Isotherm model; Kinetic model; Mangrove charcoal; Regeneration

1. Introduction

Organic and inorganic pollutants have been major concerns in environmental contamination, where mining, manufacturing, and industrialization have been degrading the water quality because of the presence of harmful compounds in effluents. Heavy metals, which include but are not limited to chromium, cadmium, and lead, continue to pose adverse effects to the well-being of both living creatures and the environment [1]. Metals' inability to degrade naturally, while being toxic, adds to the environmental load and harm [2]. Phenol and phenolic compounds have also been impacting the health of the environment persistently. Phenol toxicological property has been contributed by the formation of organic and free radical species and by its high reactivity, which accounts for its persistence and possible carcinogenic properties [3]. Different remediation techniques have been developed in the removal of these pollutants, which include but are not limited to phytoremediation, adsorption, ion-exchange, coagulation, precipitation, flocculation, and ultra-filtration among other electrochemical/chemical methods [2].

* Corresponding author.

Adsorption processes proved to be innovative and cost-effective in the removal of pollutants, where adsorbates, which range from zeolites, biochar, hydrochar, and activated carbon, are produced from a variety of raw materials that are typically from agricultural and municipal wastes in order to promote sustainability. Activated carbon (AC), which is conventionally produced through physical preparation or chemical activation, is one of the most commonly used adsorbents because of its high removal capacity and ease of production. Direct chemical activation processes proved to be more energy-efficient as both carbonization and activation processes are employed at lower temperatures. Chemical impregnation, such as potassium hydroxide, zinc chloride, and phosphoric acid activation, not only improves product properties but also contributes to production efficiency. Potassium hydroxide (KOH) has been widely used in the activation of charcoal production because of its capability to produce activated carbon with well-developed porosity and high surface area. However, this activation is usually a low yield of production. Hence, the need to establish careful handling to prevent the negative setbacks, which overturn its efficiency in manufacturing high-quality activated carbon [4]. Zinc chloride ($ZnCl_2$) is another commonly used chemical for activating carbon, it is reported in the published literature that using a higher amount of $ZnCl_2$ often results in low yield, high surface area, and consequently, better adsorption properties [5]. Phosphoric acid (H_3PO_4) is also a widely used chemical in chemical activation for activating carbon. Basaleh and Al-Malack [6] investigated the use of activated carbon obtained from municipal solid waste to remove methylene blue, used phosphoric acid to activate carbon, and reported that temperature and concentration of (H_3PO_4) were the major influencers in the activation process.

A study by Paryanto et al. [7] who investigated the preparation of AC from mangrove waste utilizing KOH chemical activation revealed that surface area and pore diameter are proportional to KOH concentration, where an increase in KOH resulted in increased surface area and pore diameter. A study by Jeyakumar and Chandrasekaran [8] who investigated the use of activated carbon obtained from marine algae to remove Pb ions, demonstrated the effect of chemical treatment on the adsorption capacity [8], where Pb(II) ions were removed with adsorption capacities of 22.93, 24.15, 23.47, and 15.62 mg/g for calcium chloride-treated, sodium carbonate-treated, sodium sulfate-treated, and commercially available *Ulva fasciata* carbons, respectively. A study by Qadeer and Khalid [9] who investigated the use of activated charcoal in the removal of Cd ions demonstrated the effect of varying parameters in the adsorption capacity of activated charcoal, where the maximum adsorption was observed at a pH of 4.0 within a 20 min contact time, with 70%–75% cadmium removal rate in a single step [9]. Research by Devi et al. [10] who investigated the use of activated carbon obtained from coconut shell in the removal of Cr demonstrated the dependence of adsorption capacity on pore size, surface area, and temperature; where activated carbon produced from coconut shell adsorbed chromium with a maximum removal efficiency of 85% at a pH value of 3. A study by Al-Malack and Dauda [11] who investigated the intake of Cd and phenol utilizing activated municipal sludge demonstrates the existence of adsorbed phenol through the increase of oxygen groups, which in the binary system with cadmium created steric hindrance that led to a drop in the cadmium removal efficiency. The study further revealed that the chemisorption from ion exchange between Cd^{2+} and phenol with the activated carbon surface functional groups.

The literature review showed that the removal of phenol in the existence of heavy metals focused mainly on the removal of heavy metals, while very few published research work focused on the removal of phenol in the presence of heavy metals in binary systems. Furthermore, there are limited sources on the use of mangrove charcoal that was activated using KOH and its application in removing phenol and heavy metals in binary systems.

Based on the published literature, and up to the knowledge of the author, the literature lacks information on the removal of phenol in the presence of metals using mangrove activated charcoal, therefore, the main objective of the current research was to investigate the effect of the presence of metals on the removal of phenol in binary systems using activated carbon obtained from mangrove charcoal. Moreover, this study aimed at the characterization of the KOH-activated mangrove charcoal and to study the effect of different important factors such as pH, adsorbent dosage, and initial concentration on the adsorption process. Furthermore, the determination of the removal efficiency and the adsorptive capacity of chromium, cadmium, lead, phenol, and phenol-heavy metal binary systems and their removal mechanisms were investigated.

2. Materials and methods

2.1. Materials

Commercial mangrove charcoal was collected, oven-dried overnight at 105°C, washed to remove dirt, and oven-dried again at the same temperature. Consequently, the dried mangrove charcoal was crushed and sieved to 2 mm particle size before being stored in glass containers. All chemical reagents used in the current study were of analytical grade and were purchased from Fisher Scientific. A small amount of HCl and NaOH (0.1 N solutions) were used for pH adjustment.

2.2. Activated charcoal production

Dried mangrove charcoal was thoroughly mixed with activation agents, namely, KOH, $ZnCl_2$, and H_3PO_4 solutions. The solution concentrations were based on the experimental design discussed in the next section. Impregnated charcoal samples were oven-dried at 110°C for 12 h to remove excess moisture. The dried samples were inserted in stainless steel pipes with two narrow port diameters. The impregnated dried charcoal sample-packed stainless steel tubes were then placed in the furnace (Nabertherm LT 5/12, Germany) and heated to the desired temperature with a heating rate of 10°C/min. After heating, the tubes were taken out from the furnace after reaching the desired holding time. Subsequently, and in order to remove the residuals, activated charcoal samples were cooled and washed continuously with de-ionized water, till the pH of the rinsed water approached a pH value between 6.5 and 7.5. Lastly,

wet activated charcoal samples were oven-dried at 105°C for overnight.

2.3. RSM for activated charcoal preparation

During the preparation of activated charcoal samples, the Box–Behnken design (BBD) was implemented, which is based on the response surface model (RSM) design technique. Moreover, statistical design software was used for designing and analyzing the experimental models, and to determine the best produced AC sample. The software generated 15 experiments with two mid-point replication for each of the three chemicals. Each model contained three parameters, namely furnace temperature, furnace holding time, and impregnation ratio; where each parameter has three equally spaced levels coded as low (–1), medium (0), and high (1). It is worth mentioning that each model has two responses, phenol removal, and yield. A deep discussion and analysis of the results can be found in the Supplementary materials under the statistical analysis heading.

2.4. Characterization of materials

2.4.1. Activated charcoal yield

The yield of raw mangrove charcoal that was activated using chemical activation is the mass percentage ratio of the produced activated charcoal to the dried raw mangrove charcoal, which was used in the activation process.

2.4.2. Elemental analysis

CHNS/O elemental analyzer (PerkinElmer 2400, USA) was used to determine the organic elemental compositions of raw and activated mangrove charcoal samples. The ash content was determined using the ASTM D2866-94 method.

2.4.3. Porosity and surface area

The surface area, including the porosity of raw and activated mangrove charcoal samples, was characterized using an automated physio-sorption unit (Micrometric, TriStar II plus V2.03, USA). The specific surface area, pore volume, and pore size were obtained through the Brunauer–Emmett–Teller (BET) analysis of the nitrogen gas adsorption–desorption isotherm data at 77°K.

2.4.4. Scanning electron microscopy

The surface morphology of raw and activated mangrove charcoal samples were examined using micrographs obtained under the scanning electron microscopy (SEM; Tescan Lyra-3, Czech Republic) that was coupled with an energy dispersive X-ray spectrometer (EDS).

2.4.5. Fourier transform infrared spectroscopy

The surface functional groups of raw and activated mangrove charcoal samples were investigated using Fourier transform infrared spectroscopy (Thermo Electron Corporation Nicolet Nexus 670 FTIR Spectrometer, USA), where aliquots of 0.5 mg samples mixed with spectrometry grade KBr at 1:1,000 (w/w) ratio were ground and pressed into 1 cm diameter pellets for analysis in the spectral range 500–4,000 cm^{-1}.

2.4.6. X-ray diffraction spectroscopy

The crystalline structure of raw and activated mangrove charcoal samples were identified using X-ray diffraction (XRD) spectroscopy (Rigaku Ultimate IV X-ray diffractometer, Japan), where the procedure was performed at 10°–80° with a step size of 0.02°/s.

2.4.7. X-ray fluorescence analysis

X-ray fluorescence analysis (XRF) is a quantitive analysis that quantifies the elements on the surface of the material, however, XRF cannot detect carbon elements. (2D Micro-XRF Bruker, USA) equipment was used for XRF analysis. The analysis was performed on raw and activated mangrove charcoal samples.

2.4.8. Thermogravimetric analysis

Thermogravimetric analysis (TGA) was used to study the effect of heat range on material weight. It mainly tests the oxidative and decomposing consistency of a substance with regard to changes in temperature. The TGA of raw material and selected produced activated carbon samples were conducted using a TGA analyzer (SDT Q600 V20.9 Build 20, USA). A small amount from raw and activated carbon was placed in an alumina crucible and exposed to pyrolysis under N_2 circulation (40 mL/min) from 30 up to 800°C with a warming amount, 10°C/min.

2.5. Adsorption experiments and analytical techniques

The adsorption experiments have been done in batch mode for singular and binary systems. The experimental procedure involved adding varying amounts of the modified activated charcoal to 100 mL of aqueous solutions that contain different concentrations of phenol, Pb, Cr_3, and Cd in a 200 mL Erlenmeyer flask at 25°C. The mixture was placed on an orbital mechanical shaker at 250 rpm to be well-mixed. A 1,000 mg/L stock solution of phenol, lead, chromium 3, and cadmium were prepared. Kinetic experiments have been done by adding 1.25 g/L of AC into 200 mL of aqueous solution contains 50 mg/L of certain pollutants, and placed on the shaker for continuous agitation for 4 h. Similarly for adsorption equilibrium experiments except that the adsorbent dosage was varied from 0.5 to 2 mg/L. This study investigated the following parameters: pH from 2 to 6, contact time from 0 to 4 h, adsorbent dosage from 0.5 to 2 g/L, and initial concentration from 20 to 100 mg/L. Phenol quantification was carried out using UV-vis spectrometer (Shimadzu, Japan), while heavy metals quantification was carried out using atomic absorption spectroscopy or AAS (PerkinElmer, 700, USA) through the direct air-acetylene flame method.

Eqs. (1) and (2) were implemented to quantify the removal and the adsorption capacity, respectively.

$$q_e\left(\text{mg/g}\right)=\left(C_0-C_t\right)\left(\frac{V}{m}\right) \quad (1)$$

$$\text{Removal efficiency}\left(\%\right)=\frac{\left(C_0-C_t\right)}{C_0}\times 100 \quad (2)$$

where q_e is the amount of pollutants adsorbed (mg) per adsorbent (g) at equilibrium conditions; C_0 (mg/L) is the initial concentration of adsorbate; C_t (mg/L) is the final concentration of adsorbate; V (L) is the volume of solution; M (g) is the mass of adsorbent.

2.6. Regeneration

The regeneration investigation was performed according to the following procedure: (1) The exhausted AC samples were washed with de-ionized water to remove excess pollutants, (2) washed AC samples were dried to remove excess moisture, (3) dried AC samples were placed in a conical flask with 5 N of NaOH or HCl and placed on the shaker for desorption for 2 h, (4) obtained AC samples were washed thoroughly with de-ionized water to reach neutral pH, this step is very important since pH value is an important parameter in solid/liquid adsorption [12] and finally (5) washed AC samples were dried and used for another cycle of adsorption. It is worth mentioning that three cycles were conducted.

3. Results and discussion

3.1. Characterization of raw and activated charcoal

During the primary investigation, the best obtained activated charcoal samples were activated by KOH and $ZnCl_2$. Phosphoric acid samples have been omitted from the discussion because of the poor obtained results in the removal of phenol.

3.1.1. Elemental analysis

Elemental analysis was conducted on raw and the best two AC samples to determine the elemental composition of the material. The analysis is called CHNS analyzer, which gives the elemental composition of the material as a percentage. Table 1, which shows the obtained results, demonstrates that the material is rich in carbon and oxygen. It is noted that the carbon content increased after activation, wherein in the case of KOH, carbon content increased around 3%, while in the case of zinc chloride, the increase was around 2%. The results can be related to the chemical activation and the release of non-carbonaceous material.

3.1.2. Porosity and surface area

The surface area and porosity were found using nitrogen adsorption–desorption isotherm at 77°K, where Table 2 shows the obtained results. Table 2 clearly shows that the surface area of the charcoal increased significantly after activation from 4.43 to 716.85 and 720.5 m^2/g for KOH and $ZnCl_2$, respectively, which indicates that the chemical activation has effectively taken place. Similar results were reported by El-Hendawy [13] where maize stalks were activated using different concentrations of KOH. When they used a similar concentration that was used in the current study, a BET surface area of 619 m^2/g was reported. Furthermore, Fu et al. [14] investigated the activation of rice husk using KOH and reported that KOH aided the development of pores by developing new pores from outside to the inside. Moreover, they related the surface area to the KOH concentration and the activation temperature. Furthermore, Nasrullah et al. [15] reported the activation of mangosteen fruit using higher concentrations of $ZnCl_2$ than the one used in the current investigation, where a BET surface of 890 m^2/g was reported. The pore size for both AC samples was 2.5 nm, which indicated mesoporous activated charcoal. The micropore area in the AC activated by KOH was higher than that activated using $ZnCl_2$, which can be attributed to the fact that AC produced by KOH was more porous in the structure that is confirmed by the SEM results. The pores volume has greatly increased for both KOH-AC and $ZnCl_2$-AC samples and reached values of 0.45 and 0.5 cm^3/g, respectively, when compared to 0.0085 cm^3/g for raw charcoal.

3.1.3. Fourier transform infrared spectroscopy

Fourier transform infrared analysis (FTIR) is an analysis utilized to determine the functional groups acting on the surface of the raw and activated carbon samples. The FTIR spectrum reported wavelengths between 400 and 4,000 cm^{-1} for raw and activated charcoal samples. As observed in Fig. 1, some of the peaks have almost similar locations but

Table 1
Elemental analysis, yield, and ash content for raw and selected AC samples

Element	Raw	KOH	$ZnCl_2$
C (%)	72.62	75.66	74.3
H (%)	1.87	1.27	1.21
N (%)	0	0	0
S (%)	0	0	0
O (%)	25.49	23.07	24.49
Ash content (%)	2.82	–	–
Yield (%)	–	50.3	60

Table 2
Surface area and pore volume for raw and activated charcoal

Parameter	Raw	KOH AC	$ZnCl_2$ AC
Specific surface area (m^2/g)	2.34	784.29	785.32
BET specific surface area (m^2/g)	4.43	716.85	720.5
Micropore area (m^2/g)	0.57	546.52	389.7
External area (m^2/g)	3.85	170.33	407.86
Pore volume (cm^3/g)	0.0085	0.45	0.5
Micropore volume (cm^3/g)	n/a	0.32	0.25
Pore size nm	7.7	2.5	2.5

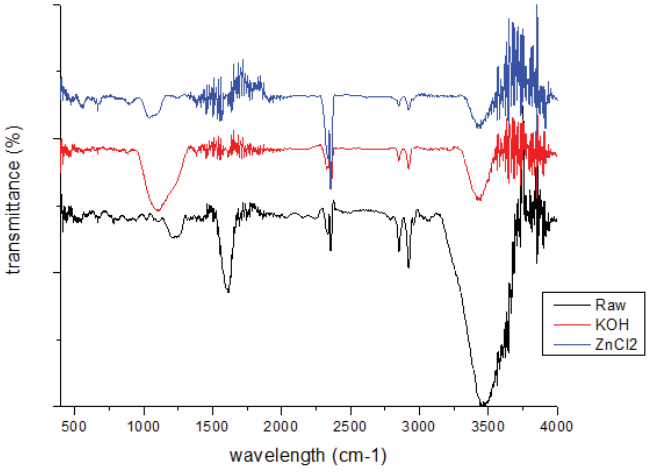

Fig. 1. FTIR plot.

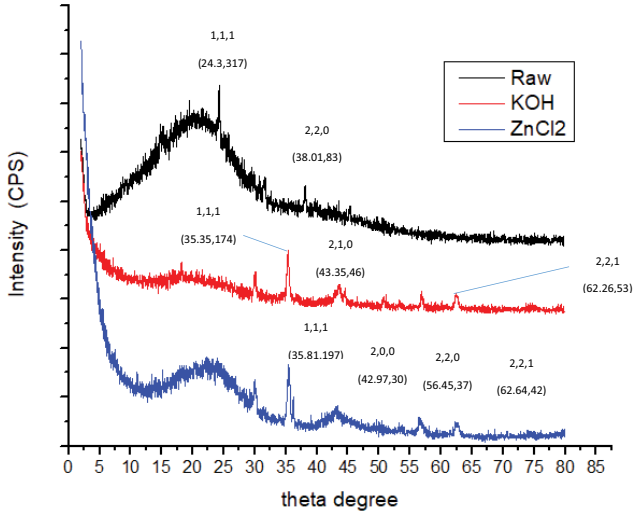

Fig. 2. XRD plot.

different transmittance. The broad bands that occur between 3,400 and 3,800 cm^{-1} for the three samples are assigned to the existence of OH stretch bond or amine N–H bond [16], while the band that occurs between 2,851 and 2,922 cm^{-1} is an indicator of the presence of C–H stretching methyl and methylene groups, or aliphatic group [13,16]. Bands between 2,339 and 2,358 cm^{-1} are assigned to carbon with a triple bond, which has a strong intensity in the $ZnCl_2$ and KOH activated carbon. The band length located between 1,736 and 1,746 cm^{-1} in $ZnCl_2$-AC is attributed to ester, and the band 1,644 cm^{-1} might be for the carbonyl group. The band length of 1,614 cm^{-1} is for the olefinic group [13]. The band length between 100 and 1,200 cm^{-1} is assigned to the C–O stretch of phenol or alcohol, which has a high intensity in the AC-KOH. The wavelength located around 650 cm^{-1} is for the alkyne C–H bond, which is found only in the $ZnCl_2$-AC sample. Finally, the wavelength between 400 and 500 cm^{-1} is assigned to Aryl disulfides S–S. It can be noted that the number of peaks has increased after activation, however, the intensity has generally been reduced.

3.1.4. X-ray diffraction spectroscopy

The crystalline structure of raw and activated carbons samples was characterized utilizing the XRD spectrometer analysis. The range of the scan was from 0° to 80°, with a step size of 0.02°/s. Fig. 2 shows the XRD profile of raw and the activated carbon samples, which demonstrates that two peaks were identified at 24° and 38°. The results indicate an amorphous structure that is typical for organic material [17]. From Fig. 2 for activated carbon with KOH, also from the profile, it can be considered as an amorphous structure with less crystalline than the raw sample. There were only three peaks that the system identified at around 35°, 43°, and 62°. Finally, for the activated carbon with zinc chloride, an amorphous structure can be identified, however, three new peaks appeared compared to the raw material. So in the AC sample that was activated using $ZnCl_2$ have four peaks, which were identified at 35°, 42°, 57°, and 63°. Close results were reported by Al-Malack and Dauda [11].

3.1.5. Scanning electron microscopy

The surface morphology was examined using an SEM, where surface topology includes sizes and shapes of pores on the outer surface of raw and activated charcoal samples. The SEM is used in parallel with the energy-dispersive X-ray spectroscopy (EDS), where EDS was used to found the elemental composition on the surface of the raw and activated carbon samples. The SEM and EDS analyses were used to determine the effect of the chemical activation process on the charcoal in terms of pores development and surface elemental composition.

Fig. 3a, which represents a raw charcoal sample, shows no sign of pores, where the figure clearly shows a smooth surface. In Fig. 3b, which represents an activated carbon sample that was activated by KOH, it can be clearly observed that the pores have developed on the surface of the sample. Fig. 3 shows that these pores vary in size and the wall structure was not retained. The development of pores is attributed to the KOH impregnation, which destroyed the lignin structure and initiated pore development [18]. The open structure is considered favorable for adsorption to maximize the surface area of the AC through enhanced diffusion [19].

Fig. 3c, which represents an activated sample that was activated using $ZnCl_2$, shows the development of cavities in the structure of the AC sample while keeping the wall structure of the material. These cavities might be formed due to the decomposition of the $ZnCl_2$ during the carbonization process [20]. The results of these images are in total agreement with the results that showed that KOH had higher removal efficiency and less yield since it had more developed pores.

As observed in Table 3, which represents the EDS results, the raw charcoal is rich in carbon and oxygen mainly, which agrees with the elemental analysis that was done and discussed earlier. Furthermore, for AC activated with KOH, the carbon content was found to increase, the oxygen was found to decrease and there are some trace elements of potassium. The increase of carbon and the decrease of oxygen can be attributed to the heating process, where the

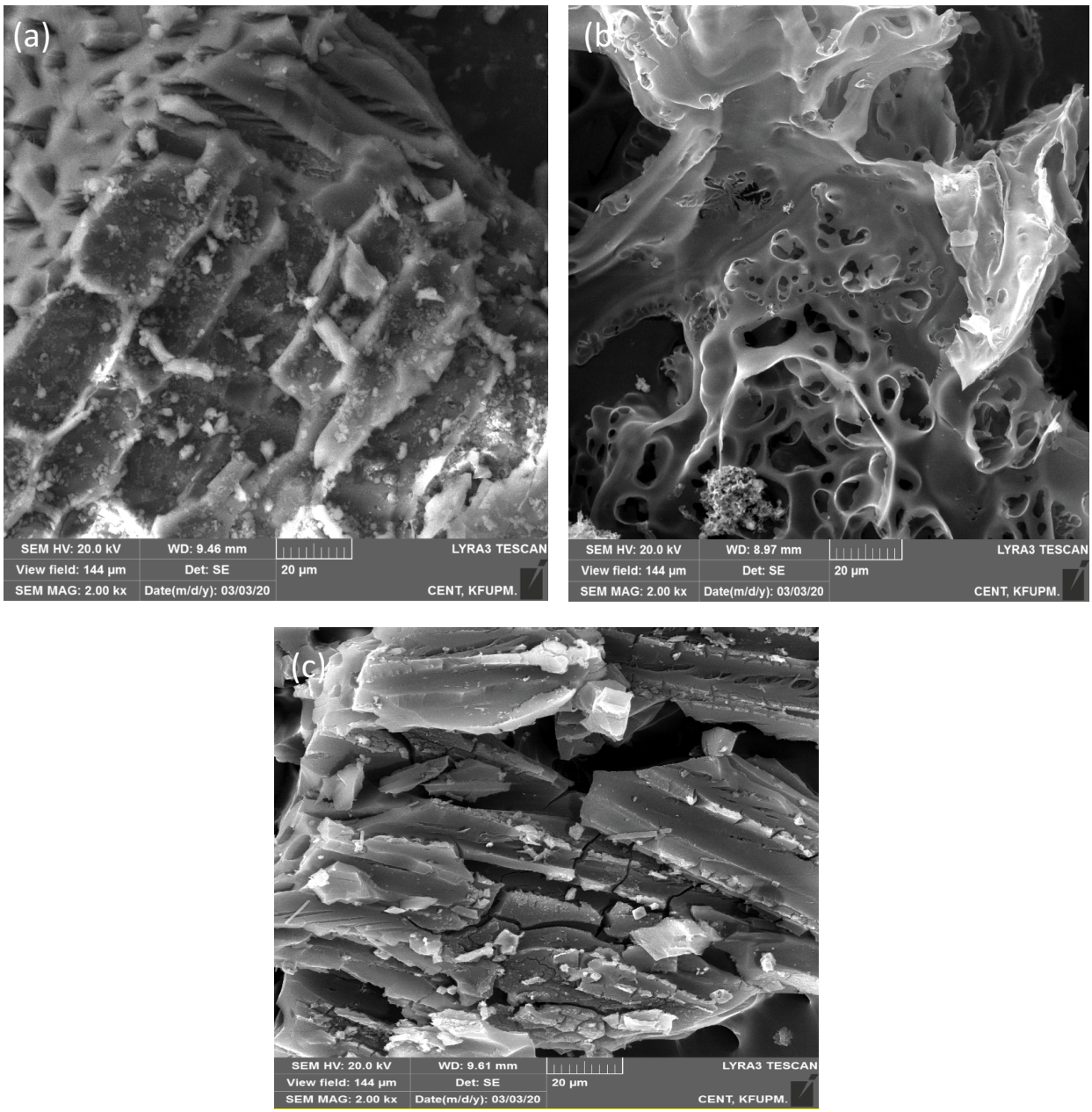

Fig. 3. SEM micrographs for (a) Raw, (b) KOH, and (c) for $ZnCl_2$.

oxygen left the carbon, and the reason behind the disappearance of potassium can be attributed to the washing process [21]. Comparable results were reported by Abdulsalam et al. [21] who investigated the ability to store natural gas from activated carbon obtained from South Africa coal. For AC activated using $ZnCl_2$, the results showed that there were decreases in carbon and oxygen due to zinc chloride impregnation that happened inside the activated carbon sample.

3.1.6. XRF analysis

The XRF analysis is a quantitative analysis that quantifies the elements on the surface of the material, however, the XRF cannot detect carbon elements. Table 4 shows the XRF results for raw and activated carbon samples. Regarding the raw charcoal, Table 4 clearly shows that the major elements on the sample surface were calcium, oxygen, chloride, and potassium. In the case of AC-KOH, the results show an increase in oxygen, silicon, sulfur, and iron. Moreover, new elements appeared such as aluminum and chromium on the surface of the sample. Similar results were reported by Hamza [22] who investigated the removal of Fe and Cr_3 using activated carbon derived from the mesquite tree. Finally, AC-$ZnCl_2$, from the table the oxygen decreased and calcium decreased compared to the raw charcoal. Further, a significant increase in the iron oxides, zinc, nickel, and chromium

elements appeared. The elements acting on the material's surface tend to improve the adsorption mechanism because they are used as a catalyst [22]. It is worth mentioning that results on TGA of raw and produced AC samples are included in the Supplementary materials.

3.2. Adsorption experiments

3.2.1. Single adsorption experiments

3.2.1.1. Effect of pH

pH is a critical factor in the adsorption of heavy metals from aqueous solutions. Since pH affects the solubility of heavy metals ions, also during the adsorption process, it might affect the ionization degree of heavy metals ions. In addition, the surface charge of the adsorbent is dependent on pH values. In the beginning, initial experiments have been done to determine the range of possible pH to be used to avoid heavy metals precipitation. In Fig. 4, it can be seen that for chromium and lead the precipitation occurs between pH 5.5 and 6, however, cadmium precipitation occurs beyond pH 8, while phenol was noticed not to precipitate at any given pH value.

To study the impact of pH on the adsorption of a single pollutant at a time, other operational factors were fixed. Adsorbent dosage was fixed at 1.25 g/L, contact time at 2 h, and initial concentration was fixed at 50 mg/L. Fig. 5 shows the impact of pH on the removal efficiency, it is clear that the effect of pH on the phenol removal was insignificant where the fluctuations were marginal. From Fig. 5, the minimum removal efficiency was around 75% at a pH value of 4, while the maximum removal efficiency was around 80% at a pH value of 5. According to Hegazy et al. [23] who studied the adsorption of phenol using activated carbon derived from *Rhazya stricta*, reported that pH affects the ionization of phenol, which could cause electrostatic repulsions between surface charge and phenolate anions in the solution [23]. Also according to Hameed and Rahman [24] who studied the removal of phenol using biomass activated carbon, reported that phenolic compounds in acidic media are in undissociated form and dispersion/diffusion interaction becomes dominant. Fig. 5 shows the impact of pH on the intake of Pb, where the minimum removal was obtained at a pH value of 2, and the maximum was obtained at a pH value of 5 and 6. Depci et al. [25] who studied the intake of Pb and Zn using activated carbon produced from apple pulp, reported that Pb ion doesn't exist beyond pH 6, where ions turn into lead hydroxide (PbOH) that causes precipitation. Also, many researchers reported that lead removal increases with the increase of pH since the density of the negative charge increases on the adsorbent surface because of the de-protonation of positively charged groups and un-protonated carboxylic groups on the surface of activated charcoal and also low hydrogen ion concentration [26,27]. Fig. 5 shows the increase in the removal efficiency of Cr

Table 3
EDS results for raw and activated charcoal samples

Sample	C (%)	O (%)	K (%)	Cl (%)	Zn (%)
Raw	68.97	31.03	0	0	0
KOH	78.43	21.15	0.42	0	0
$ZnCl_2$	66.64	30.18	0	2.31	0.87

Table 4
XRF results for raw and activated charcoal samples

Element	Raw	AC KOH	AC $ZnCl_2$
O (%)	27.35	47.98	25.25
Si (%)	2.62	16.84	0
S (%)	3.75	11.08	3.21
Cl (%)	13.74	0	13.46
K (%)	10.2	0	0
Ca (%)	38	4.34	4.78
Ti (%)	1.46	0	0
Fe (%)	1.68	5.75	31.38
Al (%)	0	8.8	0
P (%)	0	0	3.3
Ni (%)	0	1	5.56
Cr (%)	0	1.61	3
Zn (%)	0	0	8.09

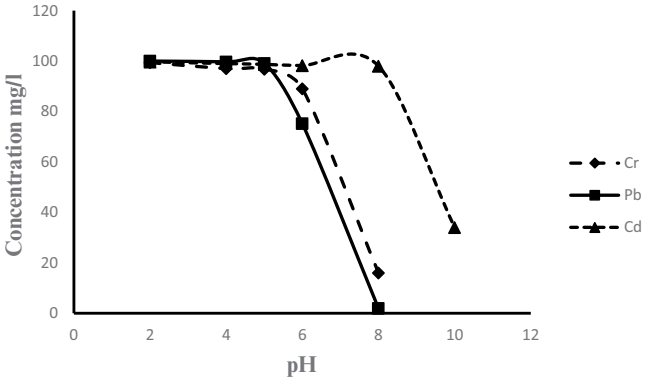

Fig. 4. Effect of pH on heavy metal solubility in aqueous solutions.

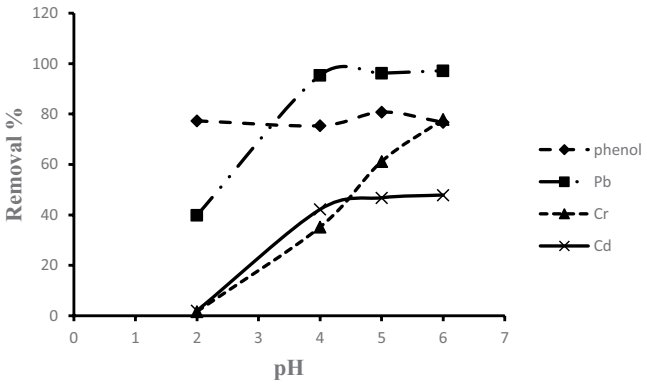

Fig. 5. Effect of pH on the removal of phenol and heavy metals in single solutions (dosage 1.25 g/L, volume 100 mL, contact time 2 h, and initial concentration 50 mg/L).

with the increase of pH. It should be noted that the removal at pH 6 includes removal from precipitation and not due to adsorption alone. Comparable results were found by Mohamed et al. [28] who studied the removal of Cd and Cr_3 using Padina waste as a low-cost adsorbent, reported that at an acidic medium, the intake was lower because of the existence of hydrogen ions competing with the chromium [28]. Finally, Fig. 5 shows that a similar trend occurred with the adsorption of Cd, where the increase of pH results in an increase in the removal efficiency of Cd. The reason behind the increased removal is also due to the presence of hydrogen ions in the acidic media, and when the pH increases the hydrogen ion reduced freeing up space for the cadmium [11].

3.2.1.2. Effect of contact time

The influence of contact time on the adsorption process performance was also investigated, where samples were collected at time intervals of 15, 30, 60, 120, and 240 min. These experiments were conducted under the following conditions: an adsorbent dosage of 1.25 g/L, pH value of 5 (optimum), and an initial concentration of 50 mg/L.

Fig. 6 shows 68% of phenol removal efficiency was obtained during the first 15 min, after which, the removal efficiency increased in steady-state reaching a maximum value of 81%, after 2 h. The figure also shows that rapid removal of Pb from the aqueous solution was observed. In the first 15 min, more than 90% removal of Pb was achieved, after which, Pb removal efficiency increased but at a very low rate reaching a maximum of 97% at the end of the experiment. Moreover, Fig. 6 shows that most of the Cr removal occurred in the first 15 min, after which, the removal started to increase slowly reaching a maximum of 60%, at the end of the experiment. Furthermore, Fig. 6 shows that the removal efficiency of around 40% of Cd was achieved in the first 15 min, after which, the removal efficiency was found to increase at lower rates and reach a value of about 50%, after 240 min of running time.

Rapid removal efficiencies that occurred at the beginning indicate the existence of many empty sites on the activated charcoal surface. Additionally, rapid removals could be attributed to the high concentrations of metals, and therefore, the contact between metal ions and the AC surface occurred rapidly. Comparable outcomes were reported by Dursun et al. [29] who studied the removal of phenol using beet pulp as an adsorbent, reported that the removal efficiency of phenol occurred in the first 80 min of the experiment.

3.2.1.3. Effect of adsorbent dosage

The effect of the adsorbent dosage on the removal of a single solute of phenol, Pb, Cd, and Cr was investigated. Due to the limited availability of the material, only small amounts of adsorbent dosage were used. The investigated dosages were 0.5, 0.75, 1.25, and 2 g/L. Batch experiments were conducted under the following conditions: pH value of 5 (optimum), initial concentration of 50 mg/L, and contact time of 2 h.

Fig. 7a shows the effect of adsorbent dosage on the removal of phenol, Pb, Cd, and Cr, which clearly demonstrates that when the adsorbent dosage was increased, the removal efficiency of contaminants increased. For phenol as an example, when the dosage was increased from 0.5 to 2 g/L the removal efficiency increased from 60% to 80%. The same trends were noticed with heavy metals, where

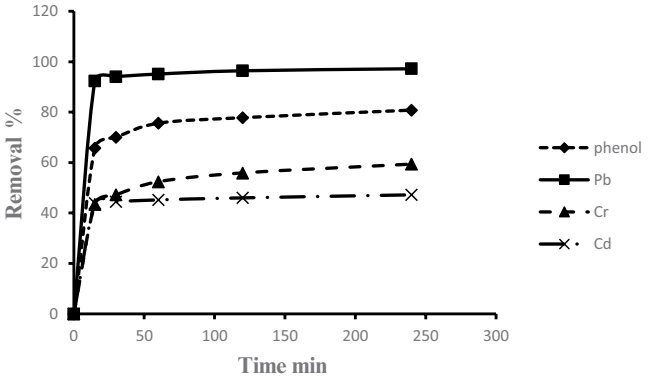

Fig. 6. Effect of contact time on removal of phenol and heavy metals in single solutions (pH 5, dosage 1.25 g/L, volume 100 mL, and initial concentration 50 mg/L).

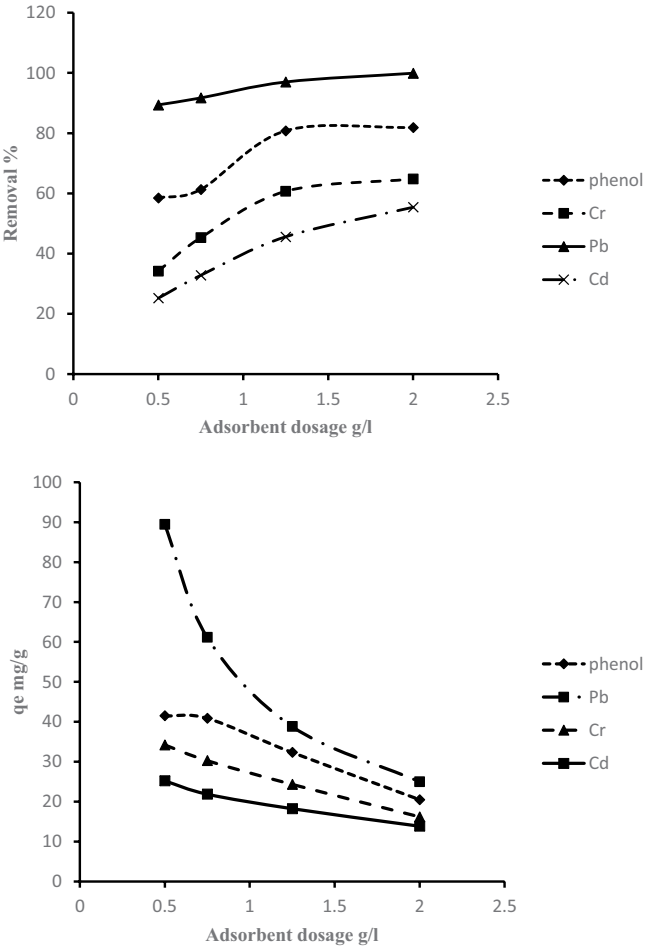

Fig. 7. Effect of adsorbent dosage on removal efficiency and adsorption capacity of phenol and heavy metals in single solutions (pH 5, volume 100 mL, contact time 2 h, and initial concentration 50 mg/L).

the increase was somewhat significant. In the case of Pb, the increase of the adsorbent dosage was not significant, because the removal was already high at a lower dosage. However, in the case of Cr and Cd, the removal almost doubled after increasing the dosage from 0.5 to 2 g/L. This phenomenon of increasing removal efficiency occurred due to the increases in the dosage of the adsorbent that will, in turn, increase the available adsorption sites [30].

Fig. 7b presents the impact of the adsorbent dosage on the adsorption capacity. It's clearly noticed that there was a decrease in the adsorption capacity when the adsorbent dosage increased, which is the opposite trend of what happened in the case of removal efficiencies. Phenol showed a decrease from 41 to 20 mg/g, Pb decreased from 89 to 24 mg/g, Cr decreased from 34 to 16 mg/g and Cd decreased from 25 to 13 mg/g. These trends of decreases are due to the empty adsorption sites that occur at a high dosage of activated charcoal with an unchanged initial concentration.

3.2.1.4. Effect of initial concentration

During the investigation of the effect of initial concentration on the removal efficiency and the adsorption capacity in a single pollutant solute system, the following parameters were fixed; pH at 5, adsorbent dose at 1.25 g/L, and contact time at 2 h, while the initial concentration was varied from 20 to 100 mg/L.

Fig. 8a shows the effect of initial concentration on the removal efficiency, where the increase in initial concentration with a fixed-dose was found to result in decreasing the removal efficiency. The drop in removal efficiency was slight in the case of phenol and Pb, where the decrease didn't exceed 20%. However, the decrease was relatively high in the case of Cr and Cd. The removal efficiency dropped in the case of Cr from 90% to 35%, while in the case of Cd, the drop was from 77% to 51%. This might be because of the AC surface sites, where at high initial concentration the adsorption process occurs at high energy [31].

Fig. 8b shows the effect of the initial concentration on the adsorption capacity. It can be noted that the increase in initial concentration has accompanied an increase in the adsorption capacity at a fixed adsorbent dose. This phenomenon is due to the driving forces, which overcomes the mass transfer between the solid–liquid phase. Also, it may be because of the increase in initial concentration, which tends to cause an increase in interaction between the AC surface and the pollutant [32].

3.2.1.5. Adsorption equilibrium isotherms

Data obtained from adsorption isotherms, which is based on the change in the initial concentration for the four pollutants, was fitted using four isotherms models, namely, Langmuir, Freundlich, Temkin, and Dubinin–Radushkevich isotherms. Linear and non-linear equations of the models are:

$$q_e = K \times C_e^{\text{bf}} \left(\text{Freundlich non-linear isotherm}\right) \tag{3}$$

$$\log q_e = \log K + \frac{1}{n}\log C_e \left(\text{Freundlich linear isotherm}\right) \tag{4}$$

$$q_e = \frac{K \times C_e}{1 + a_L \times C_e}\left(\text{Langmuir non-linear isotherm}\right) \tag{5}$$

$$\frac{1}{q_e} = \frac{1}{q_m \times K}\left(\frac{1}{C_e}\right) + \frac{1}{q_m}\left(\text{Langmuir isotherm}\right) \tag{6}$$

$$q_e = \frac{RT}{b_T}\ln\left(A_T \times C_e\right)\left(\text{Temkin non-linear isotherm}\right) \tag{7}$$

$$q_e = B_T \ln A_t + B_T \ln C_e,\ B_T = \frac{RT}{b_T}\left(\text{Temkin linear isotherm}\right) \tag{8}$$

$$q_e = q_D \exp\left(-B_D\left[RT \times L_D\left(1 + \frac{1}{C_e}\right)\right]^2\right) \tag{9}$$

$$\left(\text{Dubinin-Radushkevich non-linear}\right)$$

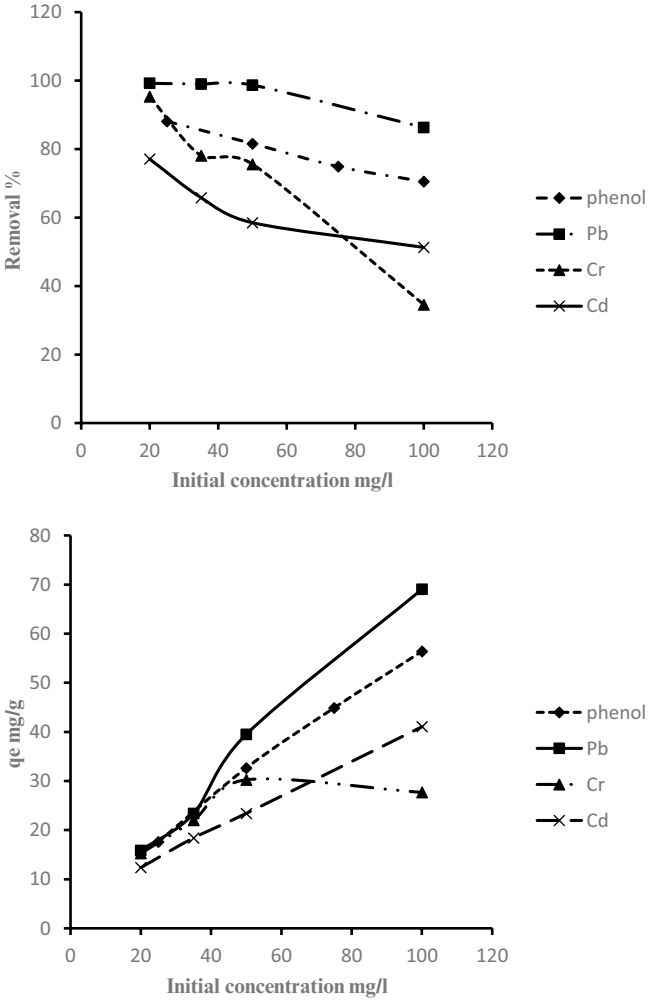

Fig. 8. Effect of initial concentration on removal efficiency and adsorption capacity of phenol and heavy metals in single solutions (pH 5, volume 100 mL, contact time 2 h, and dosage 1.25 g/L).

$$\ln q_e = \ln q_D - 2B_D RT \ln\left(1+\frac{1}{C_e}\right) \quad \text{(Dubinin-Radushkevich linear isotherm)} \tag{10}$$

Figs. 9a–c show the equilibrium isotherms for Langmuir and Freundlich, respectively. Table 5 shows the important isotherm parameters. It can be observed that phenol adsorption by the prepared AC has fitted well to the Freundlich isotherm model, with a correlation coefficient (R^2) of 0.997, which was slightly more than the Langmuir model, which gave an (R^2) of 0.993. The results suggest that the intake of phenol occurred in a multilayer of the surface of the produced AC. The high n (2) value, which was bigger than 1, indicates that the conditions, in which the adsorption experiments were conducted, were favorable [29]. Similar results were reported by Dursun et al. [29].

In the case of Pb, the adsorption fitted well to the Langmuir isotherm model, which gave a correlation coefficient of 0.96 in comparison to 0.63 in the Freundlich isotherm model. That indicates that the adsorption of Pb on the prepared AC surface occurred in a monolayer over all the active sites [33], where the maximum calculated adsorption capacity was 96.15 mg/g. Similarly, in the case of Cr, where the adsorption fitted the Langmuir isotherm that resulted in a correlation coefficient (R^2) value of 0.71 compared to 0.22 in the case of the Freundlich isotherm model, which indicated that the adsorption process occurred in a monolayer on the produced AC surface. Comparable results were mentioned by Maneechakr and Mongkollertlop [34] who studied the adsorption of several heavy metals using activated palm kernel. Finally, data obtained on Cd adsorption was determined to fit better the Langmuir isotherm model than the Freundlich isotherm model. Similar results were reported by Kedirvelu et al. [35] who investigated the adsorption of Cd on the surface of activated carbon obtained from coconut. Data obtained from the adsorption isotherms were also fitted for Temkin and D–R isotherms models, however, both isotherms didn't fit well the data. The results of the two isotherms can be found in the Supplementary materials. Non-linear models didn't show a better result than the linear model, so it was omitted from the discussion.

3.2.1.6. Adsorption kinetics

The rate at which adsorption reaches equilibrium is called adsorption kinetics. Adsorption kinetics are very important models to understand adsorption efficiency. In order to understand the mechanisms, the obtained data were fitted by pseudo-first-order, pseudo-second-order, and intra-particle diffusion kinetic models. The following equations represent the kinetics models: (the non-linear model plots and data can be found in Supplementary materials):

First-order:

$$\log\left(q_e - q_t\right) = \log\left(q_e\right) - \frac{k_1}{2.303} t \ \text{(linear)} \tag{11}$$

$$q_t = \left(q_e - e^{(-k_1 \times t)}\right) \text{(non-linear)} \tag{12}$$

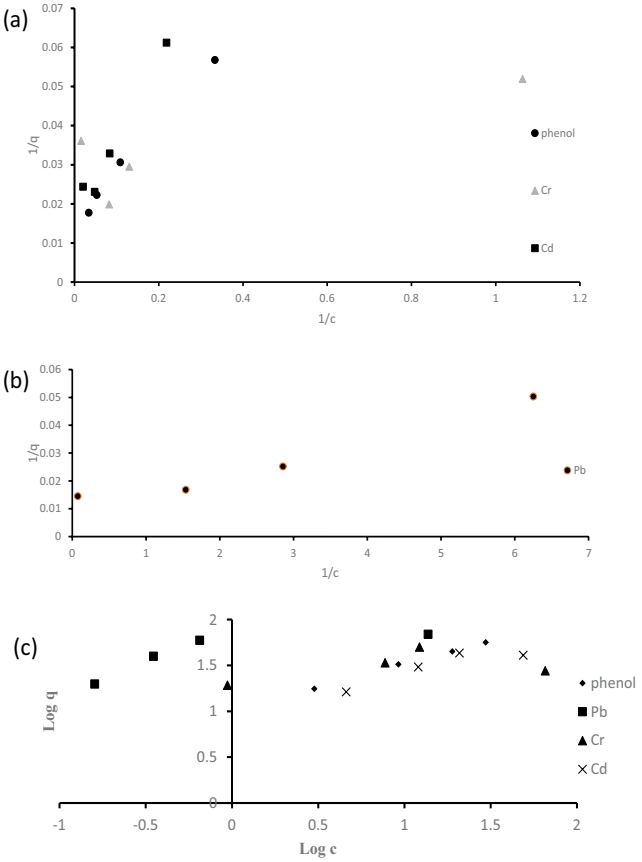

Fig. 9. Isotherms of single solute system for (a and b) Langmuir and (c) Fruendlich.

Table 5
Important isotherm parameters in singular systems

Pollutant	Freundlich			Langmuir		
	N	k_F (mg/g (L/mg)$^{1/n}$)	R^2	q_m (mg/g)	K_L (L/mg)	R^2
Phenol	1.97	10.25	0.997	65.7	0.12	0.993
Pb	4.39	44.14	0.632	96.15	1.70	0.960
Cr	9.29	24.43	0.220	37.03	1.18	0.709
Cd	2.45	10.03	0.819	59.17	0.08	0.974

Second-order:

$$\frac{t}{q_t} = \frac{1}{k_2 q_e^2} + \frac{1}{q_e} t \left(\text{linear}\right) \tag{13}$$

$$q_t = \frac{k_2 \times q_e^2 \times t}{1 + k_2 \times q_e \times t} \left(\text{non-linear}\right) \tag{14}$$

Intra-particle diffusion:

$$q_t = K_i t^{0.5} + C \tag{15}$$

where (q_e) is the theoretical equilibrium adsorption capacity (mg/g) obtained from the plot, (q_t) is adsorption capacity (mg/g) at any time (t) obtained from the experimental data, k_1 is the pseudo-first-order rate constant (min^{-1}), k_2 is the pseudo-second-order rate constant (g/mg min), K_i is the intra-particle diffusion rate constant (mg/g $min^{0.5}$).

It worth mentioning that the non-linear form of pseudo-first-order was used because the linear form didn't fit the data Figs. 10a–c show the results of pseudo-first, second-order, and intra-particle diffusion kinetic models. Moreover, Table 6 shows important parameters for the kinetic models obtained from the graphs. Fig. 10a clearly shows that all the pollutants didn't fit the pseudo-first-order linear model except in the case of Pb, where the correlation coefficient was 0.98. However, the calculated q_e was not very close to the experimental q_e, in the case of Pb. It can be demonstrated in Fig. 10b that all the pollutants fitted well pseudo-second-order. In the case of phenol, the obtained R^2 was 0.99 with a calculated q_e of 32.15 mg/g and experimental q_e of 31.68 mg/g, which indicates the closeness of the values. Cadmium also was determined to fit the second-order model, where a correlation coefficient (R^2) was 0.99, a calculated q_e of 24.44 mg/g, and an experimental q_e of 24.48 mg/g. The rest of the pollutants were also determined to fit the pseudo-second-order model in terms of the correlation coefficient, calculated, and experimental q_e values. The intra-particle diffusion model showed in Fig. 10c, where it can be observed that phenol, Pb, and Cr adsorption occurred in two stages, while Cd adsorption occurred in one stage. The first stage indicates that the adsorption occurred only on the activated charcoal surface, while the second stage indicates internal adsorption.

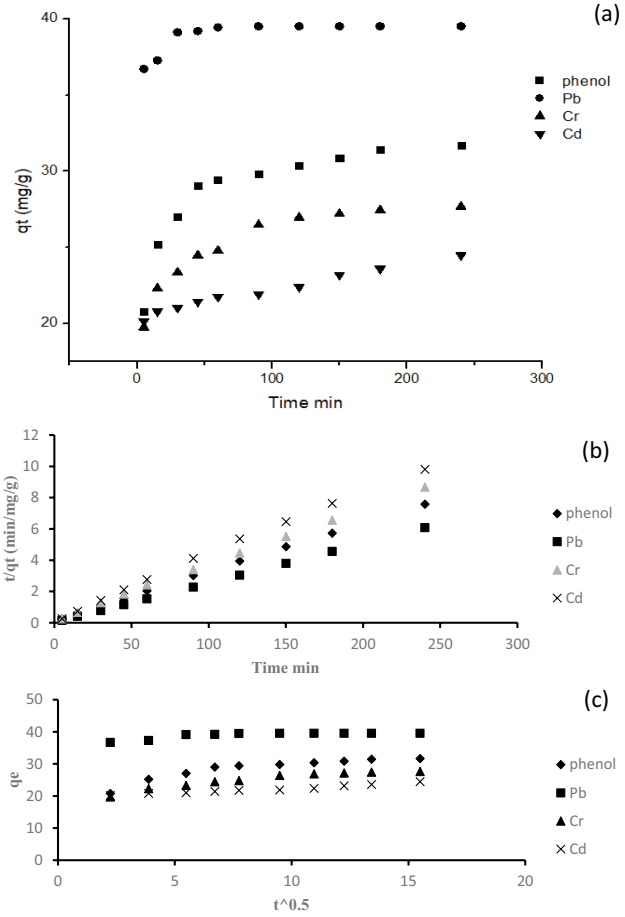

Fig. 10. Kinetic models for singular solution systems for: (a) pseudo-first-order (non-linear), (b) pseudo-second-order, and (C) intra-particle diffusion.

Based on the findings, it can be concluded that the pseudo-second-order kinetic model can describe phenol, Pb, Cr, and Cd in single solute adsorption on the surface of activated charcoal. Based on the obtained results, the adsorption mechanism was chemisorption, which includes electron interchange between the pollutants ions and the functional groups on the AC surface. Similar results were obtained by Ma et al. [36] who investigated phenol's adsorption using powdered AC. Bohli et al. [37] who investigated the intake of heavy metals on the surface of activated carbon produced from olive stones reported that the intake of heavy metals followed the pseudo-second-order model.

3.2.2. Binary adsorption

3.2.2.1. Effect of heavy metal concentration

Effects of initial concentration variations of heavy metals on the removal efficiency of phenol were investigated through fixing phenol concentration (50 mg/L) and changing concentrations of heavy metals, namely, Pb, Cr, and Cd. Moreover, other operational parameters were fixed such as pH (5) and adsorbent dose (1.25 g/L). An initial run of phenol alone at the above-mentioned parameters was conducted, where a removal efficiency of 81% was achieved at the end of the experiment.

Fig. 11 demonstrates the impact of changing Pb concentration on phenol and Pb's removal efficiency in a binary system. Fig. 11 demonstrates that activated charcoal showed more affinity toward Pb than phenol. The removal of phenol wasn't affected much by the presence of Pb even at higher Pb concentration. At low Pb concentration (10–30 mg/L), the phenol removal was found to be 78%, compared to 81% when Pb was absent, however, the removal efficiency of Pb was almost 99%. At Pb concentration of 100 mg/L, phenol removal was noticed to drop to 71%, while Pb removal efficiency was 78%. Phenol was slightly affected in the presence of Pb, even with the increase of Pb initial concentration.

That might be due to the different main mechanisms for the removal of Pb and phenol, where the Pb removal happen mainly due to the interaction with the carboxylic group and secondary by diffusion due to its small hydrated ionic radius which is around 0.401 Å, while phenol removal mainly happens by diffusion because at pH 5 phenol appears in the undissociated form and secondary by the interaction with aromatic ring and carbonyl groups [38]. A schematic of the removal of Pb can be found in the Supplementary materials.

Fig. 12 shows the relation between phenol and Cr removal efficiencies compared to the change in Cr initial concentration. At lower Cr concentrations between 10 and 20 mg/L, the removal of Cr was higher than phenol, also phenol removal efficiency was not affected significantly at these concentrations, where phenol removal efficiency reached a value of 78% when compared to 81% when Cr was absent. Fig. 12 also shows that at higher Cr concentrations, the drop in the removal efficiencies of phenol and Cr were significant. Phenol removal efficiency dropped to 66%, at a Cr concentration of 100 mg/L. Moreover, Cr intake was found to drop significantly in the presence of phenol, when the results are compared to those obtained on the removal of Cr in the absence of phenol. For example, at a Cr concentration of 50 mg/L, the removal efficiency in the absence of phenol was 75%, while it was 54% when phenol was added. Lach et al. [39] who studied the removal of Cr in the existence of phenol using activated carbon, reported that the existence of phenol affected the adsorption of Cr negatively, due to phenol competition over the oxides groups on the surface of the activated carbon [39].

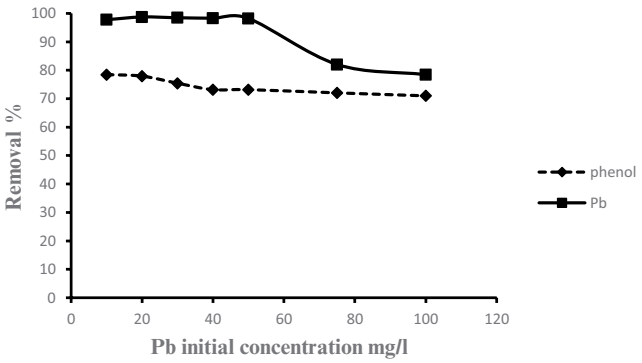

Fig. 11. Effect of initial concentration variations of Pb on removal efficiencies of phenol and Pb in binary systems (pH 5, dosage 1.25 g/L, volume 100 mL, contact time 2 h, and phenol initial concentration 50 mg/L).

Fig. 13 demonstrates the impact of changing initial concentrations of Cd on the removal efficiencies of phenol and Cd. The results clearly indicated that the produced activated charcoal showed more affinity toward phenol when compared to Cd. It is noticed that throughout the variation of Cd concentration, the removal of phenol was almost steady. However, increasing the initial concentration of Cd had an essential impact on the removal efficiency of Cd. The results clearly indicate that there was a reduction in the removal of Cd in the presence of phenol when the results are compared with those obtained on the removal of Cd in the absence of phenol. Comparable results were mentioned by Al-Malack and Dauda [11] and Arcibar-Orozco et al. [38] where they attributed such phenomenon where phenol creates a steric hindrance for cations to adsorb on specific oxygenated groups.

3.2.2.2. Adsorption equilibrium

The obtained experimental results from the binary adsorption were fitted using Langmuir, Freundlich, Temkin, and Dubinin–Radushkevich isotherms. The best two model parameters can be found in Table 7, which were obtained from Fig. 14.

From Figs. 14c and d, it was observed that phenol adsorption in binary systems with heavy metal was determined to fit well Freundlich isotherm better than Langmuir, the correlation coefficients were 0.998 and 0.983, for Freundlich and Langmuir, respectively. The results were similar to the results obtained in the singular system, where phenol also followed Freundlich isotherm that indicates the adsorption process occurred in multilayers. Regarding the obtained (n) values, which indicate the adsorption intensity, it can be noted that the intensity was higher than the one obtained in singular systems. The highest n value obtained was 3.2 for phenol with Cd, which indicates a higher affinity for phenol. Similar results were reported by Al-Malack and Dauda [11] and Arcibar-Orozco et al. [38]. The graphs for Temkin and D-R isotherms can be found in the Supplementary materials. The plotted data showed that the D–R isotherm didn't fit the data and Temkin isotherm well fitted the data; however, the binding energy constant was negative that indicates an endothermic reaction that's why the Temkin isotherm couldn't describe the adsorption equilibrium.

Figs. 14a and b shows Langmuir and Freundlich isotherms for heavy metals with phenol. For Pb, the Langmuir isotherm fitted the data with an R^2 of 0.782 compared to 0.695 for Freundlich isotherm, which means that the adsorption of

Table 6
Pseudo first- and second-order and intra-particle diffusion kinetics parameters in singular systems

Pollutant	Pseudo-first-order				Pseudo-second-order				Intra-particle diffusion	
	k_1 (1/min)	q_e (mg/g)	R^2	$q_{e,\exp}$ (mg/g)	k_2 (L/g min	q_e (mg/g)	R^2	$q_{e,\exp}$ (mg/g)	R^2	K_i (mg/g min$^{0.5}$)
Phenol	0.937	28.57	0.73	31.68	0.006	32.15	0.99	31.68	0.80	0.70
Pb	0.259	38.93	0.98	39.52	0.05	39.68	1	39.52	0.60	0.19
Cd	0.133	22.08	0.87	24.48	0.007	24.44	0.99	24.48	0.90	0.58
Cr	0.104	25.05	0.84	27.68	0.007	28.16	0.99	27.68	0.97	0.31

Pb occurred in monolayer. It is worth mentioning that similar results were obtained during the singular adsorption. Also, it was noted the q_m in the binary model increased from 96.15 mg/g in the singular to 138.89 in competitive adsorption with phenol, which indicates a higher affinity to Pb than phenol. For Cr, it was noticed that the data also fitted well Langmuir isotherm with an R^2 of 0.967. Compared to the singular adsorption experiment, which also fitted Langmuir

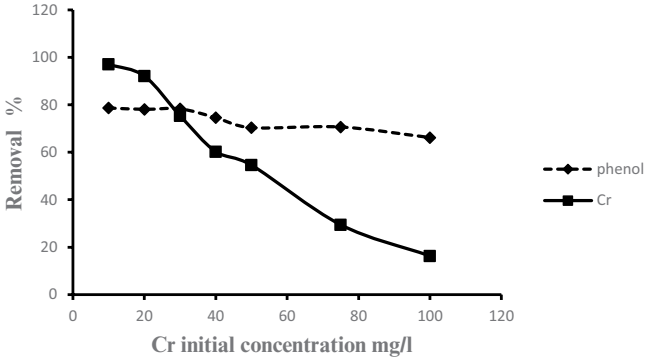

Fig. 12. Effect of initial concentration variations of Cr on removal efficiencies of phenol and Cr in binary systems (pH 5, dosage 1.25 g/L, volume 100 mL, contact time 2 h, and phenol initial concentration 50 mg/L).

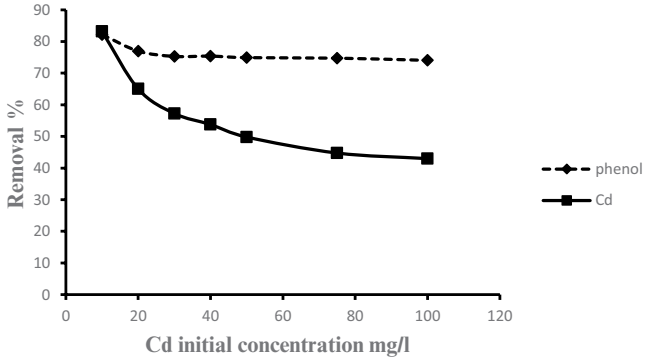

Fig. 13. Effect of initial concentration variations of Cd on removal efficiencies of phenol and Cd in binary systems (pH 5, dosage 1.25 g/L, volume 100 mL, contact time 2 h, and phenol initial concentration 50 mg/L).

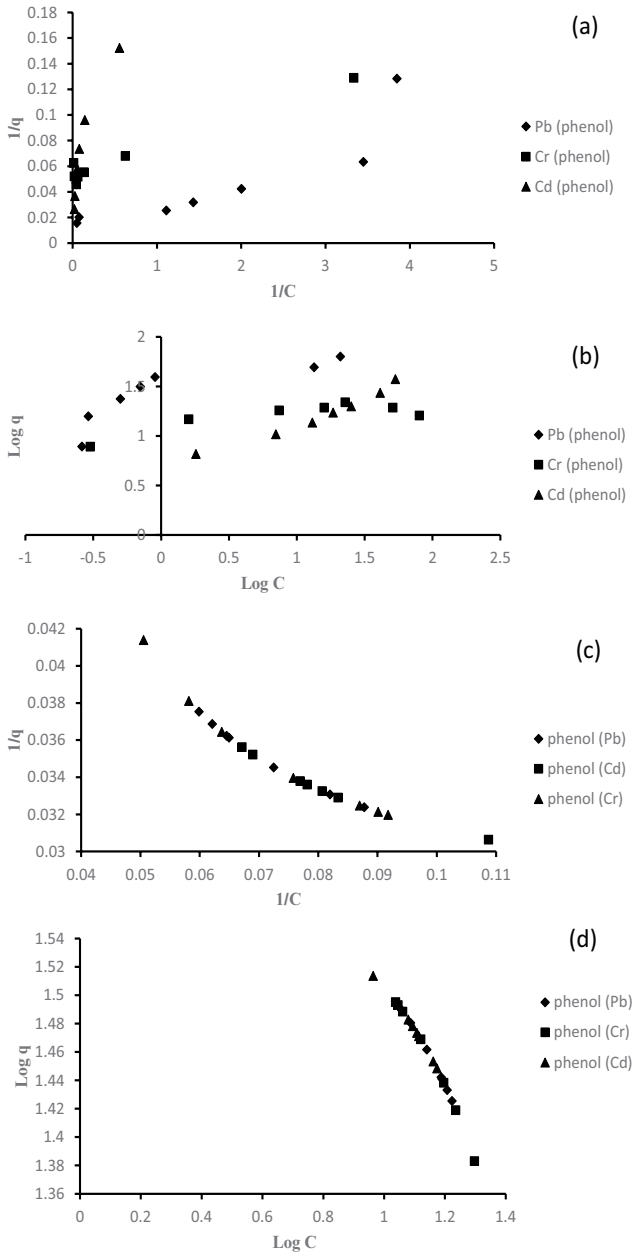

Fig. 14. Binary isotherms for (a and c) Langmuir and (b and d) Fruendlich.

Table 7
Isotherm important parameters in binary systems

Pollutant	Freundlich			Langmuir		
	N	k_F (mg/g (L/mg)$^{1/n}$)	R^2	q_m (mg/g)	K_L (L/mg)	R^2
Phenol (Pb)	2.6	79.06	0.996	20.79	0.26	0.983
Phenol (Cr)	2.4	85.5	0.987	19.68	0.24	0.952
Phenol (Cd)	3.2	65.31	0.987	23.31	0.37	0.953
Pb (phenol)	3	24.54	0.695	138.89	0.31	0.782
Cr (phenol)	7.15	11.48	0.647	19.04	2.28	0.967
Cd (phenol)	2.01	4.28	0.959	23.01	0.2	0.877

isotherm, the q_m has dropped from 37 to 19.04 mg/g in the binary system with phenol. Finally, for Cd, the Freundlich isotherm well-fitted the data with an R^2 of 0.952. It is worth mentioning that in the singular adsorption, Cd fitted the Langmuir model. The change in the adsorption isotherm behavior indicated that the adsorption of Cd with phenol happened in multilayer due to the competition between them [35].

3.2.2.3. Adsorption kinetics

Experimental data for the binary systems were fitted with the intra-particle diffusion, pseudo-first, and second-order kinetics model. The kinetic models, as mentioned before, will indicate the adsorption mechanism. Eqs. (11)–(13) were used. The important model parameters are listed in Table 8 (the non-linear model plots and data can be found in Supplementary materials).

It worth mentioning that the non-linear form of pseudo-first-order was used because the linear form didn't fit the data. Fig. 15 shows that phenol in the binary system behaved in a trend that is similar to the case of a singular adsorption experiment. The results indicate that phenol adsorption in binary system fitted well pseudo-second-order model. Chromium with phenol also fitted pseudo-second-order model with a correlation coefficient of 0.99, which is similar to the trend that occurred in the singular system. Gupta and Balomajumder [40] reported analogous results for the competitive adsorption of phenol and chromium using AC produced from tea waste [40]. Furthermore, Pb with phenol fitted well the pseudo-second-order model with an R^2 of 1, with a calculated q_m of 23.64 mg/g, while the experimental q_e was having a value of 23.6 mg/g. Lastly, Cd with phenol also fitted well the pseudo-second-order model, where similar results were reported by Al-Malack

Table 8
Important kinetic model parameters in binary systems

Pollutant	Pseudo-first-order				Pseudo-second-order				Intra-particle diffusion	
	k_1	q_e (mg/g)	$q_{e,exp}$ (mg/g)	R^2	k_2	q_e (mg/g)	$q_{e,exp}$ (mg/g)	R^2	R^2	K_i (mg/g min$^{0.5}$)
Phenol (Pb)	0.116	26.7	28.96	0.84	0.0092	29.23	28.96	0.99	0.81	0.5
Pb (Phenol)	0.143	23.23	23.6	0.98	0.9	23.64	23.6	1.0	0.50	0.1
Phenol (Cr)	0.158	29.26	30.8	0.9	0.015	30.96	30.8	0.99	0.76	0.4
Cr (Phenol)	0.052	15.75	20.48	0.68	0.0034	20.08	20.48	0.99	0.96	0.6
Phenol (Cd)	0.180	29	30.1	0.89	0.016	30.49	30.1	0.99	0.88	0.3
Cd (Phenol)	0.057	12.98	13.6	0.94	0.043	13.66	13.6	0.99	0.61	0.1

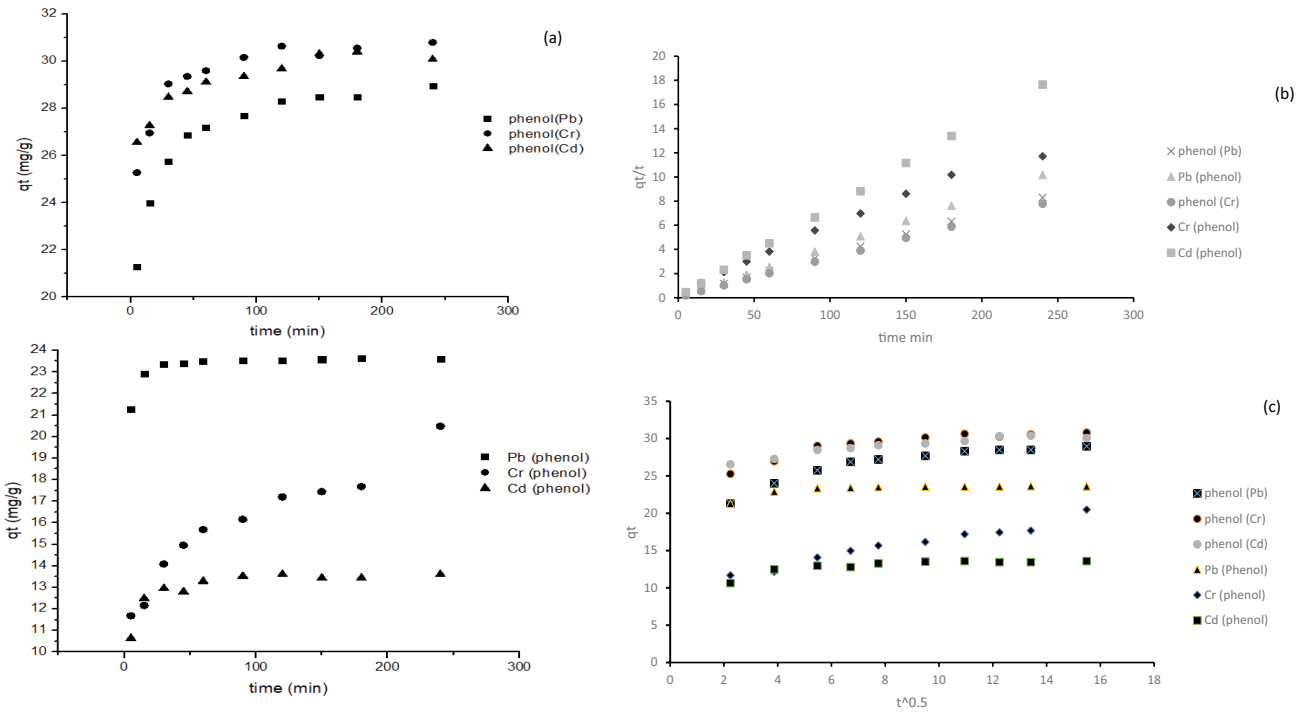

Fig. 15. Kinetic models for: (a) pseudo-first-order (non-linear), (b) pseudo-second-order, and (c) intra-particle diffusion.

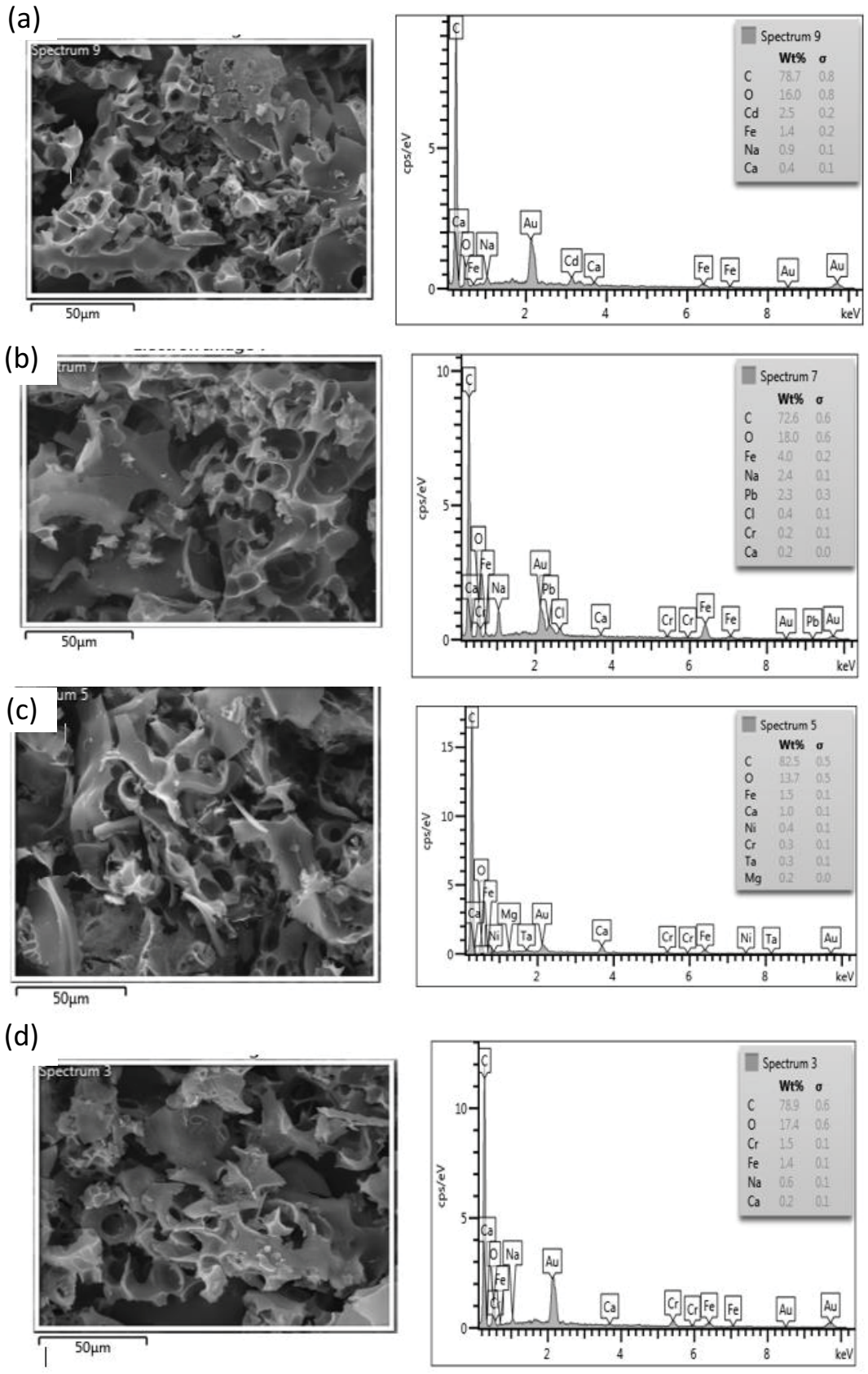

Fig. 16. SEM/EDS of AC loaded with (a) Cd, (b) Pb, (c) Phenol, and (D) Cr.

and Dauda [11]. It can be concluded based on the pseudo-second-order model that fitted all the experimental data, that the adsorption mechanism is chemisorption, which is similar to the obtained mechanism in a singular system.

3.2.3. SEM/EDS of loaded activated charcoal

The SEM/EDS analysis was done after the activated charcoal was loaded with the pollutants in the singular system, where the results of the EDS analysis can be observed in Fig. 16. From Fig. 16a, it can be observed that the sample was loaded with Cd. Moreover, Fig. 16a also shows that the oxygen element was reduced, which might be attributed that Cd interacted with oxygen functional groups existent on the surface of the produced AC [11]. Fig. 16b shows an AC sample loaded with Pb, which clearly shows that lead was present in the sample. Additionally, the reduction of the C element could be attributed to the interaction of Pb with the carboxylic groups. Furthermore, Fig. 16c shows an AC sample that was loaded with phenol, which demonstrates an increase of the carbon element since phenol is organic. Finally, Fig. 16d shows an AC sample loaded with Cr as proof of Cr adsorption. From the results, the prepared AC adsorbent has a higher affinity toward phenol, lead, and chromium and a lower affinity towards Cd.

3.2.4. Regeneration

The regeneration experiments of the exhausted AC samples were done to investigate the practicality of reusing the exhausted AC. The chemicals that were utilized during the investigation were sodium hydroxide (NaOH) and hydrochloric acid (HCl), where these chemicals were used because of their ability to reduce Van Der Waals force [41]. The regeneration experiments were done for the binary system at optimum conditions. The results of the removal efficiency of the initial run and three cycles can be found in Table 9. Phenol is acidic in nature, so when NaOH is added to the exhausted AC loaded with phenol it should disturb the stability of phenol. It can be demonstrated from the adsorption–desorption cycle of phenol using NaOH was more effective than the use of HCl. This phenomenon might be because of the reaction between phenol and sodium that results in the creation of sodium salt of phenol which eases the desorption from the AC surface [42,43]. A schematic diagram of the mechanism of NaOH regeneration can be found in the Supplementary materials. However, for heavy metals, the use of HCl was more effective in the desorption process than NaOH, which can be due to the ion exchange mechanism between hydrogen ions and metal ions [44]. A schematic diagram of the mechanism of HCl regeneration can be found in the Supplementary materials. Tang et al. [45] who studied the removal mechanism of Cd and Pb using activated carbon, reported similar results in the desorption of Pb and Cd using HCl, where he found that the desorption capacity decreased with more cycles.

4. Conclusions

Mangrove charcoal was chemically activated using KOH and $ZnCl_2$, where the best-obtained sample was found to be AC activated using KOH that was utilized in the adsorption batch experiments throughout the investigation period. The adsorption experiments included singular systems namely, phenol, Pb, Cr, and Cd. Also, binary systems included phenol with Pb, phenol with Cr, and phenol with Cd. The raw and activated charcoal samples were characterized using elemental analysis, porosity and surface area, FTIR, TGA, XRD, SEM/EDS, and XRF. Effects of pH, initial concentration, AC dosage, and contact time on the adsorption process performance were investigated with the singular systems only. The optimum conditions such as pH and AC dosage obtained from the singular systems were fixed and used in the binary systems. The adsorption affinity was towards Pb > phenol > Cr > Cd in the singular system. Heavy metals intake was determined to be heavily dependent on the system pH, unlike phenol that showed little sensitivity towards pH variations. Different equilibrium isotherms were utilized to fit the data, namely, Freundlich, Langmuir, Temkin, and D–R isotherms. Phenol was found to fit well to Freundlich isotherm, however, all heavy metals fitted the Langmuir model. Also, all the data well fitted pseudo-second-order kinetic model, while intra-particle diffusion indicated that the adsorption occurred in two stages, except for Cd. In binary systems, phenol concentration was fixed and optimum conditions of pH and AC dosage were applied. In the case of phenol with Pb, the produced AC showed a higher affinity toward Pb, however, in the case of phenol with Cr and phenol with Cd, the produced AC showed a higher affinity toward phenol. It was noticed that the increase in heavy metal concentration negatively impacted phenol adsorption due to the competition on the available surface sites of the prepared AC. The data for phenol in a binary system was

Table 9
Removal efficiency after regeneration of AC samples

	Phenol + Pb NaOH		Phenol + Cr NaOH		Phenol + Cd NaOH		Phenol + Pb HCl		Phenol + Cr HCl		Phenol + Cd HCl	
Pollutant	Phenol %	Pb %	Phenol %	Cr %	Phenol %	Cd %	Phenol %	Pb %	Phenol %	Cr %	Phenol %	Cd %
Initial	81.1	97.2	83	74.6	82.9	63.3	76.3	98.2	83.3	72	82.3	58.3
Cycle 1	76.7	90.7	78.3	53	75.8	48.2	53.6	96.5	71.7	69	65.6	51.6
Cycle 2	73.9	82.4	76.8	51.3	74.7	24	45.2	92.4	64	63.7	51.3	50.4
Cycle 3	67.5	75.6	69.6	42.6	72.2	18.1	38.7	88.9	46.5	58.3	39	47.3

determined to fit Freundlich isotherm as in the case of singular systems, which indicated that the adsorption trend didn't change, also Pb and Cr fitted well Langmuir isotherm similar to their singular systems. On the other hand, Cd was found to fit Freundlich isotherm in the binary adsorption systems. Data obtained on kinetics was found to fit the pseudo-second-order kinetic model, which indicates chemisorption. The regeneration study was performed in three cycles on the produced AC samples that were used during the binary system investigation, where NaOH and HCl were used for desorption of the contaminants. The obtained results indicated that NaOH was more effective than HCl in phenol desorption that was attributed to sodium salt formation, however, HCl was found to be better than NaOH in the desorption of heavy metals that was attributed to the ion competition between hydrogen and metal ions.

Acknowledgments

The authors would like to express their gratitude to King Fahd University of Petroleum and Minerals (Dhahran, Saudi Arabia) for the technical and financial supports that were provided during the investigation.

References

[1] P. Bharti, Heavy Metals in Environment, 1st ed., Lambert Academic Publishing GmbH & Co. KG, Saarbrucken, Germany, 2012.
[2] P. Gautam, R. Gautam, S. Banerjee, M. Chattopadhyaya, J. Pandey, Heavy Metals in the Environment: Fate, Transport, Toxicity and Remediation Technologies, D. Pathania, Ed., Heavy Metals: Sources Toxicity And Remediation Techniques, Nova Science, New York, USA, 2016, pp. 101–130.
[3] A. Abd Gami, M. Shukor, K. Khalil, F. Dahalan, A. Khalid, Phenol and its toxicity, J. Environ. Microbiol. Toxicol., 2 (2014) 11–24.
[4] T.S. Hui, M.A.A. Zaini, Potassium hydroxide activation of activated carbon: a commentary, Carbon Lett., 16 (2015) 275–280.
[5] P.E. Hock, M.A.A. Zaini, Activated carbons by zinc chloride activation for dye removal – a commentary, Acta Chim. Slovaca, 11 (2018) 99–106.
[6] A.A. Basaleh, M.H. Al-Malack, Utilization of municipal organic solid waste for production of activated carbon in SA, Arabian J. Sci. Eng., 43 (2018) 3585–3599.
[7] W. Paryanto, A. Wibowo, D. Hantoko, M.E. Saputro, Preparation of activated carbon from mangrove waste by KOH chemical activation, IOP Conf. Ser.: Mater. Sci. Eng., 543 (2019) 12087–12095, doi: 10.1088/1757-899X/543/1/012087.
[8] R.P.S. Jeyakumar, V. Chandrasekaran, Adsorption of lead(II) ions by activated carbons prepared from marine green algae: equilibrium and kinetics studies, Int. J. Ind. Chem., 5 (2014) 5–10, doi: 10.1007/s40090-014-0010-z.
[9] R. Qadeer, N. Khalid, Removal of cadmium from aqueous solutions by activated charcoal, Sep. Sci. Technol., 40 (2005) 845–859.
[10] V. Devi, A. Jahagirdar, Z. Ahmed, Adsorption of chromium on activated carbon prepared from coconut shell, Int. J. Eng. Res. Appl., 2 (2012) 362–370.
[11] M.H. Al-Malack, M. Dauda, Competitive adsorption of cadmium and phenol on activated carbon produced from municipal sludge, J. Environ. Chem. Eng., 5 (2017) 2718–2729.
[12] Q. Li, Y. Qi, C. Gao, Chemical regeneration of spent powdered activated carbon used in decolorization of sodium salicylate for the pharmaceutical industry, J. Cleaner Prod., 86 (2015) 424–431.
[13] A.N.A. El-Hendawy, An insight into the KOH activation mechanism through the production of microporous activated carbon for the removal of Pb^{2+} cations, Appl. Surf. Sci., 255 (2009) 3723–3730.
[14] Y. Fu, Y. Shen, Z. Zhang, X. Ge, M. Chen, Activated bio-chars derived from rice husk via one- and two-step KOH-catalyzed pyrolysis for phenol adsorption, Sci. Total Environ., 646 (2019) 1567–1577.
[15] A. Nasrullah, A. Bhat, M.H. Isa, M. Danish, A. Naeem, N. Muhammad, T. Khan, Efficient removal of methylene blue dye using mangosteen peel waste: kinetics, isotherms and artificial neural network (ANN) modelling, Desal. Water Treat., 86 (2017) 191–202.
[16] A.B.D. Nandiyanto, R. Oktiani, R. Ragadhita, How to read and interpret FTIR spectroscope of organic material. Indonesian J. Sci. Technol., 4 (2019) 97–118.
[17] E. Köseoğlu, C. Akmil-Başar, Preparation, structural evaluation and adsorptive properties of activated carbon from agricultural waste biomass, Adv. Powder Technol., 26 (2015) 811–818.
[18] O. Oginni, K. Singh, G. Oporto, B. Dawson-Andoh, L. Mcdonald, E. Sabolsky, Influence of one-step and two-step KOH activation on activated carbon characteristics, Biores. Technol. Rep., 7 (2019) 1002–1022, doi: 10.1016/j.biteb.2019.100266.
[19] C. Djilani, R. Zaghdoudi, F. Djazi, B. Bouchekima, A. Lallam, A. Modarressi, M. Rogalski, Adsorption of dyes on activated carbon prepared from apricot stones and commercial activated carbon, J. Taiwan Inst. Chem. Eng., 53 (2015) 112–121.
[20] L. Demiral, C.A. Şamdan, H. Demiral, Production and characterization of activated carbons from pumpkin seed shell by chemical activation with $ZnCl_2$, Desal. Water Treat., 57 (2015) 2446–2454.
[21] J. Abdulsalam, J. Mulopo, B. Oboirien, S. Bada, R. Falcon, Experimental evaluation of activated carbon derived from South Africa discard coal for natural gas storage, Int. J. Coal Sci. Technol., 6 (2019) 459–477.
[22] N.A.E. Hamza, Adsorption of metals (Fe(II), Cr(III) and Co(II)) from aqueous solution by using activated carbon prepared from mesquite tree, Sci. J. Anal. Chem., 1 (2013) 12–20, doi: 10.11648/j.sjac.20130102.12.
[23] A.K. Hegazy, N.T. Abdel-Ghani, G.A. El-Chaghaby, Adsorption of phenol onto activated carbon from *Rhazya stricta*: determination of the optimal experimental parameters using factorial design, Appl. Water Sci., 4 (2013) 273–281.
[24] B. Hameed, A. Rahman, Removal of phenol from aqueous solutions by adsorption onto activated carbon prepared from biomass material, J. Hazard. Mater., 160 (2008) 576–581.
[25] T. Depci, A.R. Kul, Y. Önal, Competitive adsorption of lead and zinc from aqueous solution on activated carbon prepared from Van apple pulp: study in single- and multi-solute systems, Chem. Eng. J., 200–202 (2012) 224–236.
[26] M. Minceva, R. Fajgar, L. Markovska, V. Meshko, Comparative Study of Zn^{2+}, Cd^{2+}, and Pb^{2+} removal from water solution using natural clinoptilolitic zeolite and commercial granulated activated carbon. Equilibrium of adsorption, Sep. Sci. Technol., 43 (2008) 2117–2143.
[27] M. Zhang, Adsorption study of Pb(II), Cu(II) and Zn(II) from simulated acid mine drainage using dairy manure compost, Chem. Eng. J., 172 (2011) 361–368.
[28] H.S. Mohamed, N. Soliman, D.A. Abdelrheem, A.A. Ramadan, A.H. Elghandour, S.A. Ahmed, Adsorption of Cd^{2+} and Cr^{3+} ions from aqueous solutions by using residue of *Padina gymnospora* waste as promising low-cost adsorbent, Heliyon, 5 (2019), 1287–1319 doi: 10.1016/j.heliyon.2019.e01287.
[29] G. Dursun, H. Çiçek, A.Y. Dursun, Adsorption of phenol from aqueous solution by using carbonised beet pulp, J. Hazard. Mater., 125 (2005) 175–182.
[30] A.A. Basaleh, M.H. Al-Malack, T.A. Saleh, Methylene Blue removal using polyamide-vermiculite nanocomposites: kinetics, equilibrium and thermodynamic study, J. Environ. Chem. Eng., 7 (2019) 103–107.

[31] A.H. Ali, Comparative study on removal of cadmium(II) from simulated wastewater by adsorption onto GAC, DB, and PR, Desal. Water Treat., 51 (2013) 5547–5558.
[32] A.S. Thajeel, M.M. Al-Faize, A.Z. Raheem, Removal of Cu^{2+} & Fe^{3+} ions from oil wells by local activated carbon in batch adsorption process, Aquat. Sci. Technol., 1 (2013) 78–94.
[33] C.S. Araújo, I.L. Almeida, H.C. Rezende, S.M. Marcionilio, J.J. Léon, T.N.D. Matos, Elucidation of mechanism involved in adsorption of Pb(II) onto lobeira fruit (*Solanum lycocarpum*) using Langmuir, Freundlich and Temkin isotherms, Microchem. J., 137 (2018) 348–354.
[34] P. Maneechakr, S. Mongkollertlop, Investigation on adsorption behaviors of heavy metal ions (Cd^{2+}, Cr^{3+}, Hg^{2+} and Pb^{2+}) through low-cost/active manganese dioxide-modified magnetic biochar derived from palm kernel cake residue, J. Environ. Chem. Eng., 8 (2020) 104–467.
[35] K. Kadirvelu, C. Namasivayam, Activated carbon from coconut coirpith as metal adsorbent: adsorption of Cd(II) from aqueous solution, Adv. Environ. Res., 8 (2004) 729.
[36] Y. Ma, N. Gao, W. Chu, C. Li, Removal of phenol by powdered activated carbon adsorption, Front. Environ. Sci. Eng., 7 (2013) 158–165.
[37] T. Bohli, A. Ouederni, N. Fiol, I. Villaescusa, Evaluation of an activated carbon from olive stones used as an adsorbent for heavy metal removal from aqueous phases, C.R. Chim., 18 (2015) 88–99.
[38] J.A. Arcibar-Orozco, J.R. Rangel-Mendez, P.E. Diaz-Flores, Simultaneous adsorption of Pb(Ii)-Cd(Ii), Pb(Ii)-phenol, and Cd(Ii)-phenol by activated carbon cloth in aqueous solution, Water Air Soil Pollut., 226 (2015) 1–10.
[39] J. Lach, E. Okoniewska, E. Neczaj, M. Kacprzak, The adsorption of Cr(III) and Cr(VI) on activated carbons in the presence of phenol, Desalination, 223 (2008) 249–255.
[40] A. Gupta, C. Balomajumder, Simultaneous adsorption of Cr(VI) and phenol onto tea waste biomass from binary mixture: multicomponent adsorption, thermodynamic and kinetic study, J. Environ. Chem. Eng., 3 (2015) 785–796.
[41] R. Berenguer, J. Marco-Lozar, C. Quijada, D. Cazorla-Amorós, E. Morallón, Electrochemical regeneration and porosity recovery of phenol-saturated granular activated carbon in an alkaline medium, Carbon, 48 (2010) 2734–2745.
[42] B. Ozkaya, Adsorption and desorption of phenol on activated carbon and a comparison of isotherm models, J. Hazard. Mater., 129 (2006) 158–163.
[43] B. Xie, J. Qin, S. Wang, X. Li, H. Sun, W. Chen, Adsorption of phenol on commercial activated carbons: modelling and interpretation, Int. J. Environ. Res. Public Health, 17 (2020) 789–802, doi: 10.3390/ijerph17030789.
[44] T.D. Šoštarić, M.S. Petrović, F.T. Pastor, D.R. Lončarević, J.T. Petrović, J.V. Milojković, M.D. Stojanović, Study of heavy metals biosorption on native and alkali-treated apricot shells and its application in wastewater treatment, J. Mol. Liq., 259 (2018) 340–349.
[45] C. Tang, Y. Shu, R. Zhang, X. Li, J. Song, B. Li, D. Ou, Comparison of the removal and adsorption mechanisms of cadmium and lead from aqueous solution by activated carbons prepared from *Typha angustifolia* and *Salix matsudana*, RSC Adv., 7 (2017) 16092–16103.

Supporting information

S1. Statistical analysis

The obtained responses for the 15 experiments for each chemical can be found in Tables S1–S3. The data were analyzed by statistical software. Transformation of the response model was carried out when required on particular responses to meet the normal distribution condition. Analysis of variance (ANOVA) was implemented to understand which parameter was significant and which was not significant; any *p*-value more than 0.05 considered insignificant. Tables S4–S9 show the ANOVA table for the three parameters and their interaction and Figs. S1–S3 shows the response surface plot that supports the ANOVA table results.

Table S4 represents the ANOVA table for KOH for phenol removal response. Clearly, observed that temperature and impregnation ratio were the most significant parameters that affected the AC activated with KOH in phenol removal. Oginni et al. [18] reported in their research that KOH concentration and activating temperature positively impacted the increase of surface area and adsorption capabilities [1]. Table S5 shows the ANOVA table for KOH for the yield response. It is observed that the three factors and their interaction were significant. These three factors negatively affected the yield, which implies that an increase in any of the factors would cause a drop in the obtained yield. That may be attributed to the gas formation because of the high temperature and holding time, and a high concentration of KOH motivates faster destruction of the carbon structure [2]. Phosphoric acid achieved the lowest phenol removal and obtained the highest yield compared to the other two chemicals, it's clear from Tables S6 and S7 that H_3PO_4 concentration was the significant factor for phenol removal and it affected it positively; holding time was the most significant factor for the yield response, which means that an increase of the holding time caused a reduction in the yield. Tables S8 and S9 show the ANOVA table for the AC activated by $ZnCl_2$; the temperature was the most significant parameter for both of the responses. Hock and Zaini [3] reported similar results who investigated the removal of methylene blue using activated carbon, he reported that high temperature with zinc chloride acts as a dehydrating agent and motivates the decomposition of carbonaceous material, this reaction also causes the creation of a porous structure that causes lower yield.

Table S1
Experimental design factors and response values for H_3PO_4 activation

Std	Run	Factor 1 furnace temperature (C)	Factor 2 chemical concentration (ratio)	Factor 3 furnace time (h)	Response phenol removal (%)	Yield (%)
6	1	800	40	1	10	66.67
4	2	800	50	2	30.62	33.33
12	3	600	50	3	25.18	16.67
5	4	400	40	1	32.47	80.00
1	5	400	30	2	28.6	90.00
10	6	600	50	1	17.39	86.67
3	7	400	50	2	21.02	90.00
11	8	600	30	3	39.87	70.00
8	9	800	40	3	33.81	30.00
15	10	600	40	2	31.7	83.33
2	11	800	30	2	38.29	30.00
14	12	600	40	2	37.46	83.33
9	13	600	30	1	38.6	93.33
7	14	400	40	3	19	90.00
13	115	600	40	2	38.1	83.33

Table S2
Experimental design factors and response values for KOH activation

Std	Run	Factor 1 furnace temperature (C)	Factor 2 chemical concentration (ratio)	Factor 3 furnace time (h)	Response Phenol Removal (%)	Yield (%)
6	1	800	2:1	1	85.78	6.67
2	2	800	1:1	2	64.88	50.00
14	3	600	2:1	2	57.23	41.67
8	4	800	2:1	3	15.54	16.67
3	5	400	3:1	2	26.97	59.33
9	6	600	1:1	1	56.16	60.00
12	7	600	3:1	3	76.21	28.33
13	8	600	2:1	2	62.7	41.67
4	9	800	3:1	2	87.27	6.67
15	10	600	2:1	2	53.5	41.67
11	11	600	1:1	3	34.14	90.00
1	12	400	1:1	2	2.21	66.67
5	13	400	2:1	1	28.29	86.67
7	14	400	2:1	3	19	56.67
10	15	600	3:1	1	82.4	50.30

Table S3
Experimental design factors and response values for $ZnCl_2$ activation

Std	Run	Factor 1 furnace temperature (C)	Factor 2 chemical concentration (ratio)	Factor 3 furnace time (h)	Response phenol removal (%)	Yield (%)
4	1	800	3:1	2	81.4	40.0
8	2	800	2:1	3	75	40.0
6	3	800	2:1	1	85.7	60.0
12	4	600	3:1	3	40.6	70.0
5	5	400	2:1	1	32.4	76.7
13	6	600	2:1	2	44.6	50
11	7	600	1:1	3	36.3	60.0
10	8	600	3:1	1	37.4	63.3
3	9	400	3:1	2	36.4	70.0
14	10	600	2:1	2	47	50.0
2	11	800	1:1	2	77.8	36.7
7	12	400	2:1	3	31.4	63.3
15	13	600	2:1	2	41.1	50.0
9	14	600	1:1	1	45.8	56.7
1	15	400	1:1	2	27.4	83.3

Table S4
KOH ANOVA phenol removal response

Source	Sum of squares	df	Mean square	*F*-value	*p*-value	
Model	8,026.27	6	1,337.71	4.20	0.0331	Significant
A-Temperature	3,916.13	1	3,916.13	12.29	0.0080	Significant
B-Concentation	1,666.38	1	1,666.38	5.23	0.0516	Significant
C-Holding time	1,450.99	1	1,450.99	4.55	0.0654	Insignificant
AB	1.40	1	1.40	0.0044	0.9487	Insignificant
AC	928.73	1	928.73	2.91	0.1262	Insignificant
BC	62.65	1	62.65	0.1965	0.6693	Insignificant
Residual	2,550.17	8	318.77			
Lack of fit	2,507.34	6	417.89	19.52	0.0495	Significant
Pure error	42.82	2	21.41			
Cor. total	10,576.43	14				

Table S5
KOH ANOVA yield response

Source	Sum of squares	df	Mean square	*F*-value	*p*-value	
Model	6,361.83	6	1,060.3	20.18	0.0002	Significant
A-Temperature	4,093.32	1	4,093.32	77.89	0.0001	Significant
B-Concentration	887.05	1	887.05	16.88	0.0034	Significant
C-Holding time	422.53	1	422.53	8.04	0.0220	Significant
AB	323.82	1	323.82	6.16	0.038	Significant
AC	584.91	1	584.91	11.13	0.0103	Significant
BC	50.20	1	50.20	0.9552	0.3570	Insignificant
Residual	420	8	52.55			
Lack of fit	420	6	70			
Pure error	0.0000	2	0.0000			
Cor. total	6,782.23	14				

Table S6
H_3PO_4 ANOVA phenol removal response

Source	Sum of squares	df	Mean square	*F*-value	*p*-value	
Model	7.66	6	1.28	2.38	0.1279	Insignificant
A-Temperature	0.0628	1	0.0628	0.1169	0.7413	Insignificant
B-Concentration	2.83	1	2.83	5.27	0.0509	Significant
C-Holding time	0.6397	1	0.6397	1.19	0.3068	Insignificant
AB	0.0030	1	0.0030	0.0055	0.9427	Insignificant
AC	3.98	1	3.98	7.42	0.0261	Significant
BC	0.1393	1	0.1393	0.2594	0.6243	Insignificant
Residual	4.30	8	0.5370			
Lack of fit	4.12	6	0.6861	7.67	0.1199	Insignificant
Pure error	0.1790	2	0.0895			
Cor. total	11.95	14				

Table S7
H_3PO_4 ANOVA yield response

Source	Sum of squares	df	Mean square	*F*-value	*p*-value	
Model	37.81	6	6.30	4.53	0.0269	Significant
A-Temperature	19.57	1	19.57	14.07	0.0056	Significant
B-Concentration	2.35	1	2.35	1.69	0.2295	Insignificant
C-Holding time	9.39	1	9.39	6.75	0.0317	Significant
AB	0.0219	1	0.0219	0.0158	0.9031	Insignificant
AC	2.61	1	2.61	1.88	0.2080	Insignificant
BC	3.87	1	3.87	2.78	0.1340	Insignificant
Residual	11.12	8	1.39			
Lack of fit	11.12	6	1.85			
Pure error	0.0000	2	0.0000			
Cor. total	48.93	14				

Table S8
$ZnCl_2$ ANOVA phenol removal response

Source	Sum of squares	df	Mean square	*F*-value	*p*-value	
Model	0.0008	6	0.0001	14.49	0.0007	Significant
A-Temperature	0.0007	1	0.0007	79.86	<0.0001	Significant
B-Concentration	7.957E-06	1	7.957E-06	0.8939	0.3721	Insignificant
C-Holding time	1.522E-06	1	1.522E-06	0.1710	0.6901	Insignificant
AB	9.040E-06	1	9.040E-06	1.02	0.3431	Insignificant
AC	7.784E-08	1	7.784E-08	0.0087	0.9278	Insignificant
BC	2.529E-08	1	2.529E-08	0.0028	0.9588	Insignificant
Residual	0.0001	8	8.901E-06			
Lack of fit	0.0001	7	0.0000	15.38	0.1940	Insignificant
Pure error	6.554E-07	1	6.554E-07			
Cor. total	0.0008	14				

Table S9
$ZnCl_2$ ANOVA yield response

Source	Sum of squares	df	Mean square	*F*-value	*p*-value	
Model	0.0002	6	0.0000	5.15	0.0187	Significant
A-Temperature	0.0002	1	0.0002	23.01	0.0014	Significant
B-Concentration	6.217E-07	1	6.217E-07	0.0815	0.7825	Insignificant
C-Holding time	0.0000	1	0.0000	4.24	0.0735	Insignificant
AB	8.639E-06	1	8.639E-06	1.13	0.3183	Insignificant
AC	0.0000	1	0.0000	1.36	0.2767	Insignificant
BC	3.524E-06	1	3.524E-06	0.4620	0.5159	Insignificant
Residual	0.0001	8	7.628E-06			
Lack of fit	0.0001	7	8.718E-06			
Pure error	0.0000	1	0.0000			
Cor. total	0.0003	14				

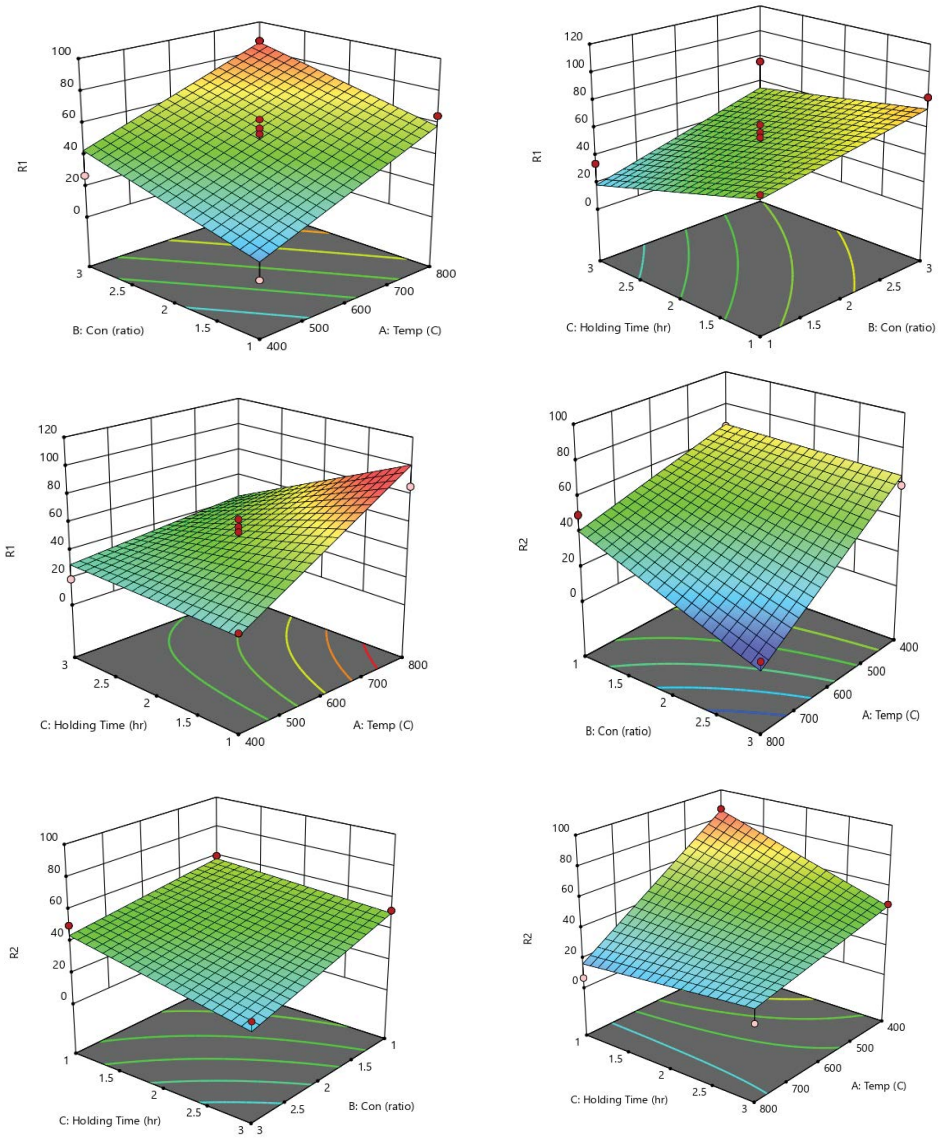

Fig. S1. 3-D response surface plot showing the interaction between various parameters for KOH activation process on phenol removal (R1) and yield (R2).

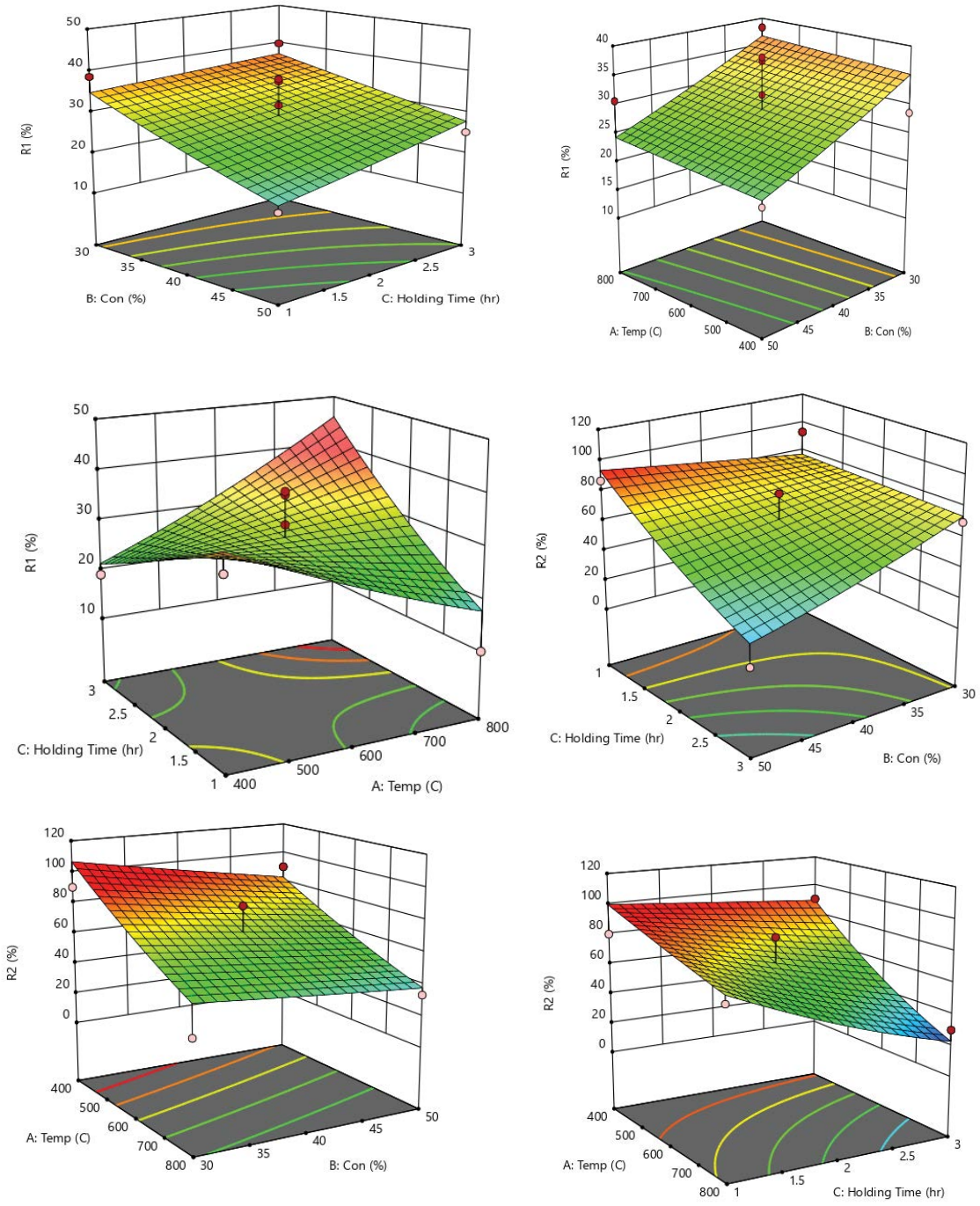

Fig. S2. 3-D response surface plot showing the interaction between various parameters for H_3PO_4 activation process on phenol removal (R1) and yield (R2).

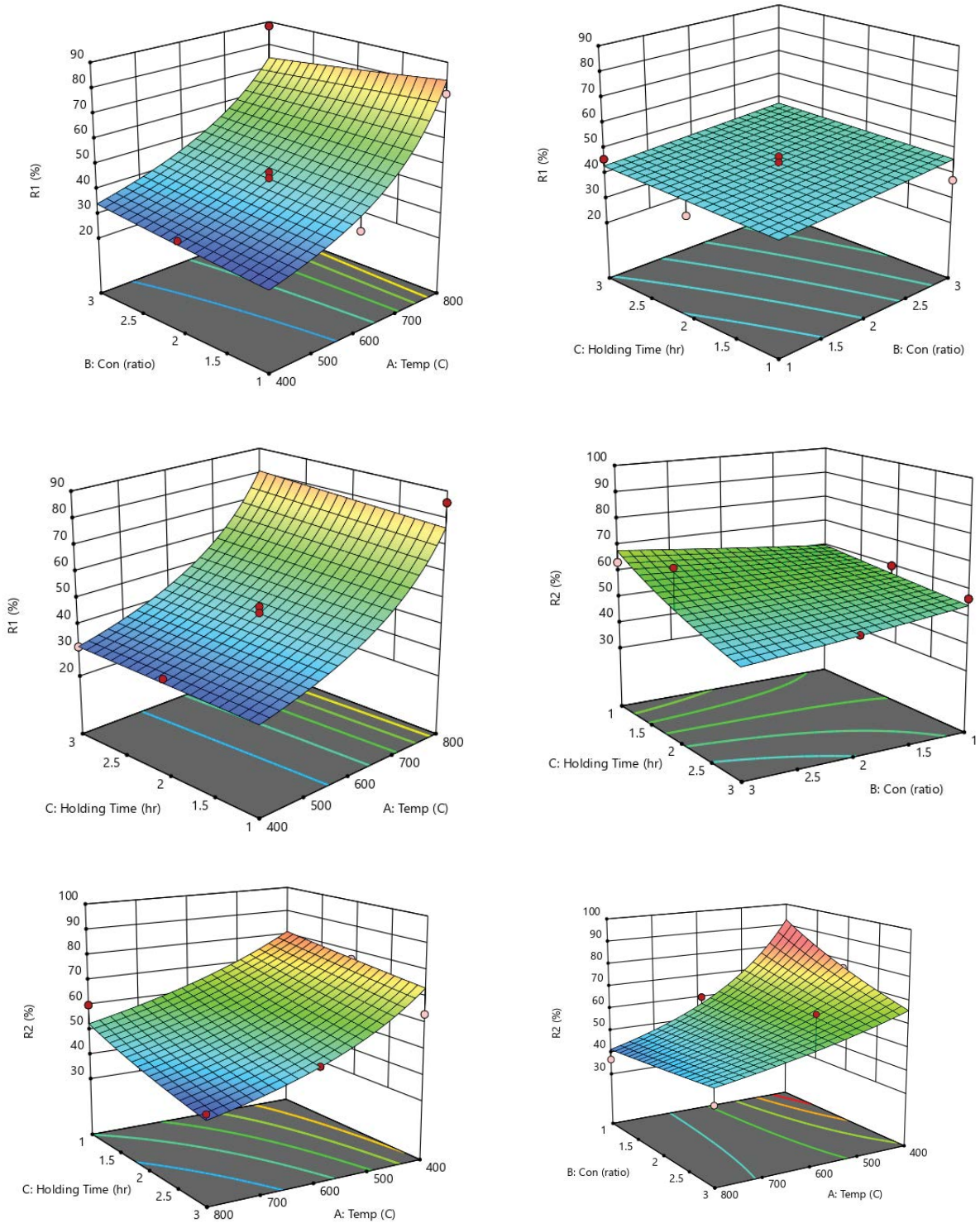

Fig. S3. 3-D response surface plot showing the interaction between various parameters for $ZnCl_2$ activation process on phenol removal (R1) and yield (R2).

S2. Binary adsorption and regeneration

Fig. S4 shows the mechanism of Pb removal.

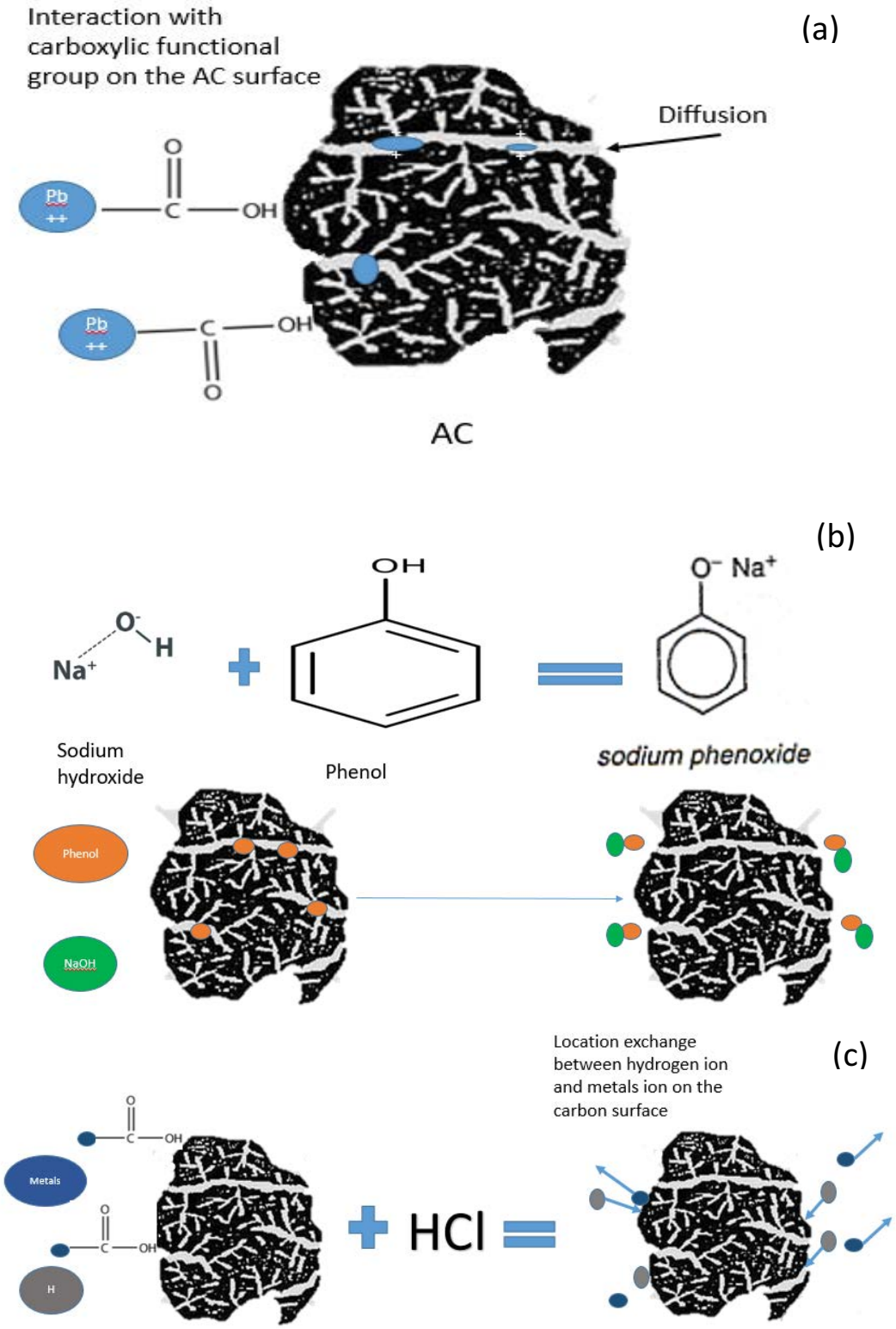

Fig. S4. Schematic diagram of: (a) Pb removal using AC-KOH, (b) phenol regeneration using NaOH, and (c) metals regeneration using HCl.

S3. Adsorption isotherms

Figs. S5–S10 shows the adsorption equilibrium isotherm using Temkin and D–R isotherm model.

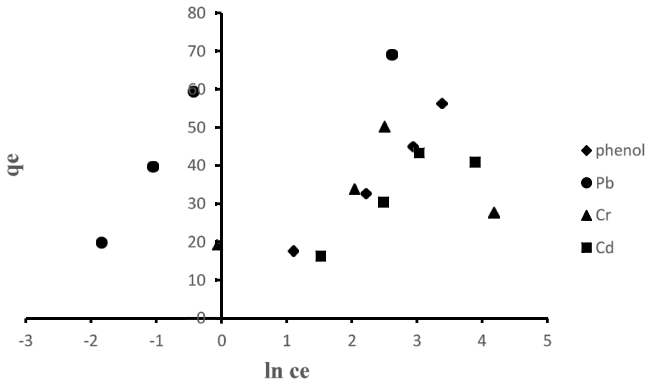

Fig. S5. Temkin isotherm for a singular solution.

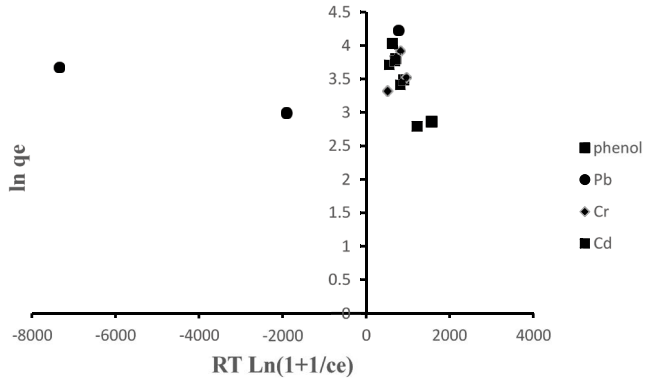

Fig. S6. D–R isotherm for a singular solution.

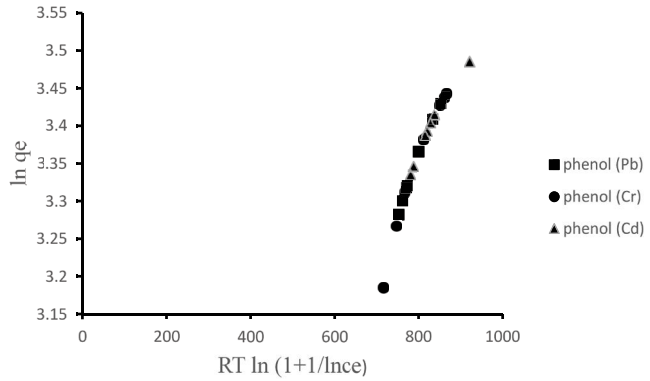

Fig. S7. D–R isotherm for phenol in a binary system.

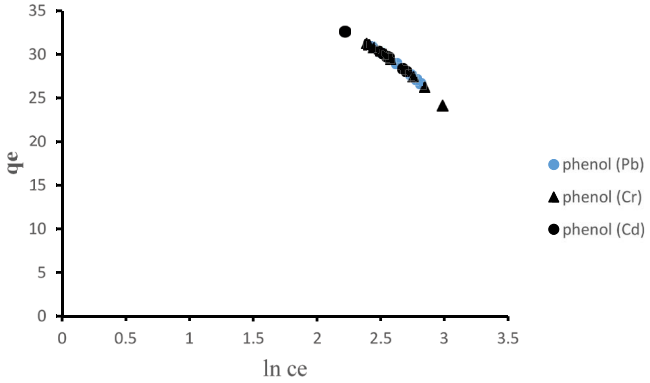

Fig. S8. Temkin isotherm for phenol in a binary system.

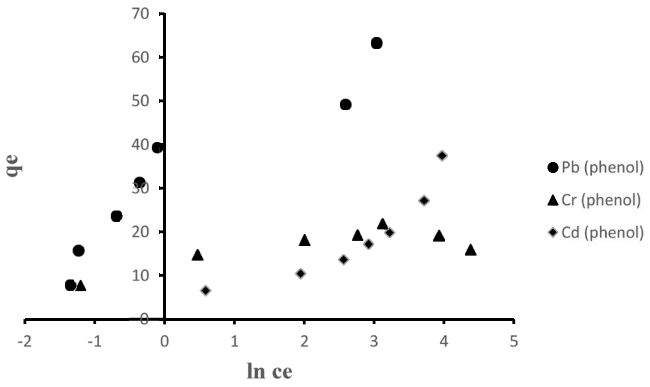

Fig. S9. Temkin isotherm for heavy metals in binary systems.

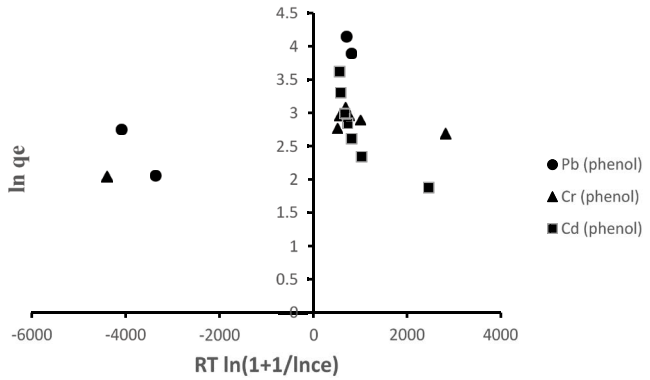

Fig. S10. D–R isotherm for heavy metals in binary systems.

S4. Adsorption kinetics

Figs. S11–S16 shows non-linear adsorption kinetics.

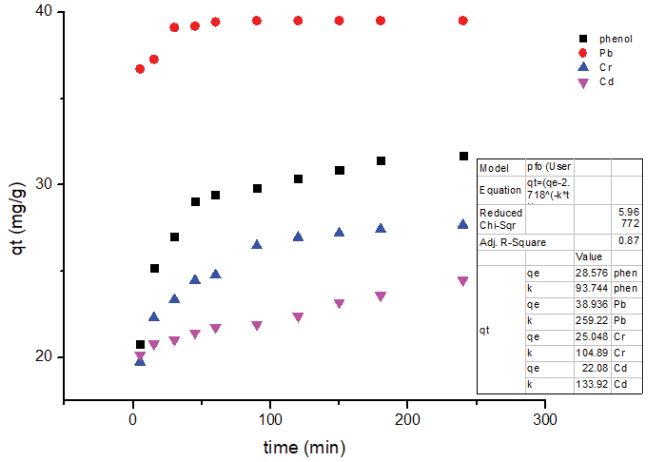

Fig. S11. PFO non-linear singular.

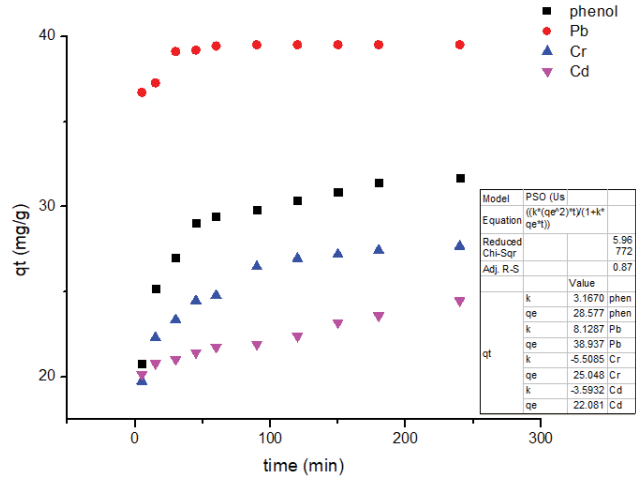

Fig. S12. PSO non-linear singular.

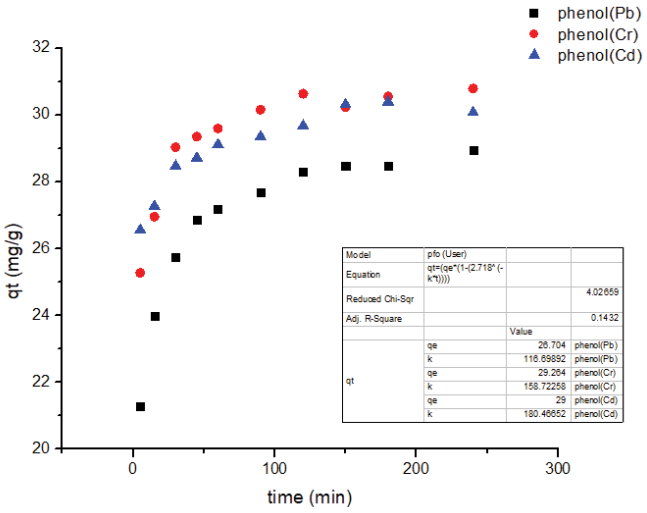

Fig. S13. PFO non-linear binary phenol with metal.

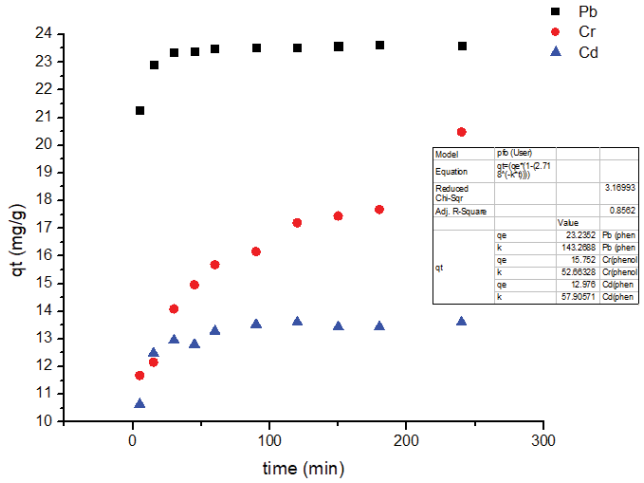

Fig. S14. PFO non-linear binary metal with phenol.

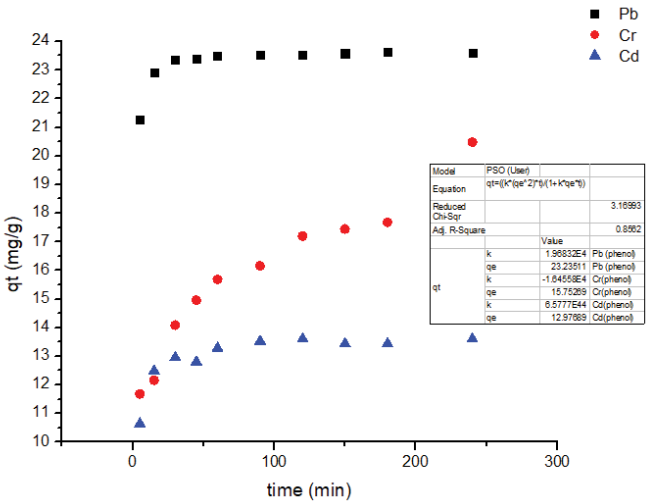

Fig. S15. PSO non-linear binary metal with phenol.

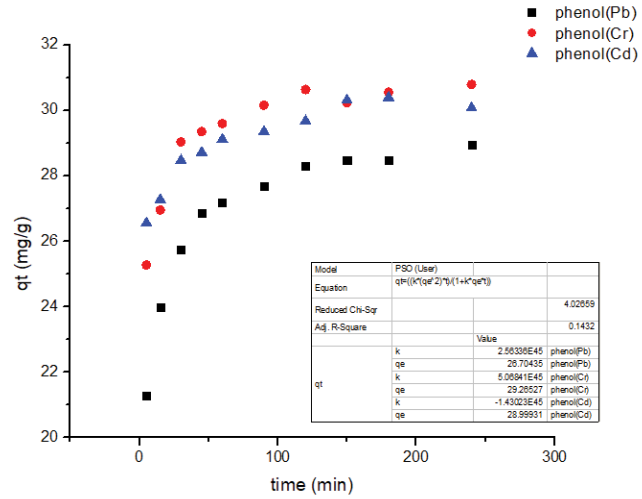

Fig. S16. PSO non-linear binary phenol with metal.

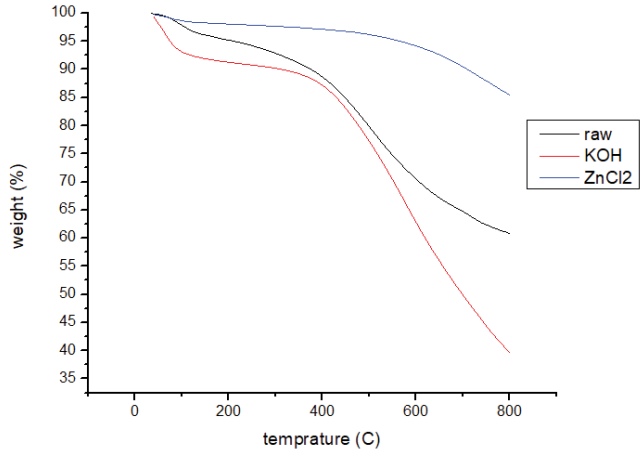

Fig. S17. TGA curve.

S5. Thermogravimetric analysis

The TGA analysis was performed on raw and produced selected activated charcoal samples. The primary target of using TGA was to visualize changes of weight with respect to heat and check the thermal stability of the material. Fig. S17 shows the thermogravimetric curve of the raw and activated charcoal. Fig. S17 shows that for raw charcoal there were three main stages of weight loss. The first stage of weight loss happened between 35°C and 170°C, which was around 5% of the total weight that is attributed to the evaporation of water molecules. The second stage occurred between 200°C and 500°C, which was around 20% of weight loss, while the final stage occurred between 600°C and 800°C. The second and third stages of weight loss were due to the gasification of organic matter and the decomposition of lignin inside the raw charcoal [4]. It is worth mentioning that the total weight loss was around 40% of the total weight.

Fig. S17 shows the three levels of weight loss for AC-KOH, where the first stage was between 35°C and 100°C. This loss, which is about 10%, is due to moisture loss that has been absorbed by the material during the washing process. The second stage was between 100°C and 400°C, where the loss was not significant. The low weight loss was attributed to the decomposition resistance of the firmly held organic volatiles such as lignin. The third stage occurred between 400°C and 800°C and the total weight loss was around 50% of the total weight. This loss was due to the destruction of the organic matter and the decomposition of some functional groups that are thermally unstable [4,5]. It can be noted that KOH-activated carbon is thermally unstable. Finally, Fig. S17 shows the TGA result of the AC-$ZnCl_2$ sample. The first stage occurred somewhere between 35°C and 100°C, accounting for 2% of the total weight loss, which was attributed to the release of moisture content. The second stage happened at 100°C and 400°C, which was negligible (less than 1%). The third stage happened between 450°C and 800°C, which was around 22%. The sharp drop was due to the decomposition and volatilization of the inorganic constituent and the infused $ZnCl_2$ that have been gained during the activation process [6]. Based on the TGA results of AC-$AnCl_2$, it can be concluded that the material was thermally stable.

References

[1] O. Oginni, K. Singh, G. Oporto, B. Dawson-Andoh, L. Mcdonald, E. Sabolsky, Influence of one-step and two-step KOH activation on activated carbon characteristics, Bioresour. Technol. Rep., 7 (2019) 1002–1022, doi: 10.1016/j.biteb.2019.100266.

[2] W. Paryanto, A. Wibowo, D. Hantoko, M.E. Saputro, Preparation of activated carbon from mangrove waste by KOH chemical activation, IOP Conf. Ser.: Mater. Sci. Eng., 543 (2019) 12087–12095, doi: 10.1088/1757-899X/543/1/012087.

[3] P.E. Hock, M.A.A. Zaini, Activated carbons by zinc chloride activation for dye removal – a commentary. Acta Chim. Slovaca, 11 (2018) 99–106.

[4] L. Muniandy, F. Adam, A.R. Mohamed, E. Ng, The synthesis and characterization of high purity mixed microporous/mesoporous activated carbon from rice husk using chemical activation with NaOH and KOH, Microporous Mesoporous Mater., 197 (2014) 316–323.

[5] G.F. Oliveira, R.C. Andrade, M.A. Trindade, H.M. Andrade, C.T. Carvalho, Thermogravimetric and spectroscopic study (TG-DTA/FT-IR) of activated carbon from the renewable biomass source Babassu, Quím. Nova, 1 (2016) 284–292.

[6] C. Li, S. Kumar, Preparation of activated carbon from un-hydrolyzed biomass residue, Biomass Convers. Biorefin., 6 (2016) 407–419.